POLITECNICO DI TORINO

Master's Degree in Engineering and Management

Master's Degree Thesis

Business case and economic analysis for Offshore Floating PV Platform

Supervisors
Prof. Giuseppe Giorgi
Prof. Emiliano Nelson Gorr

Candidate
Ulugbek Yuldoshboev

July 2025

Abstract

This thesis develops and applies a comprehensive, data-driven techno-economic framework for floating photovoltaic (FPV) systems, combining high-resolution reanalysis inputs with class-specific performance and cost parameters to inform project design and site selection. Our Python model ingests ERA5 solar-radiation, wave-height, bathymetry and wind-speed fields alongside CMEMS wave-period data to compute annual energy yield for three FPV platform classes—robust HDPE-pipe rafts (Class 1), modular floats (Class 2) and pontoon systems (Class 3)—each corrected by empirically-derived yield factors. Capital-expenditure (CAPEX) sub-components (moorings, platforms, solar modules, electrical balance-of-system) and operational-expenditure (OPEX) are calculated explicitly and then scaled with power-law exponents ($\alpha = \beta = 0.9$) to capture economies of scale. To demonstrate geographical sensitivity, the model is applied to two contrasting sites, one in the semi-enclosed Mediterranean Sea and one in a more exposed North Sea location—where local water depths, nearest-port distances, and meteorological regimes differ markedly. For each site and platform class, we quantify CAPEX, OPEX, levelized cost of energy (LCOE), net present value (NPV) and payback time across 1,10,100 MW scales. Comparative analysis reveals that Mediterranean conditions (lower wave heights, higher irradiance) favor higher yields and shorter payback for Class 2 rafts, whereas North Sea deployments require more robust Class 3 pontoons but benefit from stronger economies of scale at large capacities. Break-even tariff thresholds are identified via sensitivity scans on energy price, and seasonal removal strategies are evaluated for their impact on OPEX and annual energy production. To streamline platform selection, we integrate a scoring system that maps site-specific environmental parameters (Hs, Tp, wind speed, and depth) into the most suitable FPV class. This automated, scoring-driven assignment ensures structural resilience and economic efficiency, offering a robust decision-support tool for rapid site screening and optimization of floating solar projects under realistic environmental and financial constraints. In the North Sea, small-scale FPV installations remain uneconomic due to limited solar irradiance, but beyond a threshold of ~50 MW the sub-linear CAPEX scaling drives NPV positive having LCOE=€70.38 for class1, LCOE=€82.91 for class 2, LCOE=€87.70 for class 3 and payback below project life.

In contrast, Mediterranean conditions yield positive NPVs even at modest capacities (1–20 MW), having LCOE=€65.84 for class1, LCOE=€77.57 for class 2, LCOE=€82.04 for class3 for Pn=1MW, and when Pn=20MW, having LCOE=€48.94 for class1, LCOE=€57.65 for class2, LCOE=€60.98 for class3 with payback times consistently under 20 years across all three platform classes. These results underscore that site-dependent environmental factors (Hs, Tp, wind speed, depth) critically govern economic viability, and that large-scale deployment is especially crucial for higher-latitude, low-irradiance locations.

Class 1 HDPE-pipe rafts represent a mid-range, “universal” solution, balancing moderate cost with solid performance across most marine conditions. Class 2 modular floats are the least expensive option—up to 20 % lower CAPEX/OPEX—but deliver slightly reduced energy output (≈ 10 % less than Class 1), making them ideal where budget is constrained and wave conditions are mild. Class 3 pontoons carry the highest CAPEX and OPEX but offer the greatest structural robustness and roughly 10 % higher annual energy yield compared to Class 1. This tool provides a robust decision-support platform for screening and optimizing FPV projects under realistic environmental, structural and economic constraints, and offers generalizable insights for accelerating floating solar integration in diverse marine settings.

Acknowledgements

I would like to express my deepest gratitude to my supervisor, Prof. Giuseppe Giorgi, for his unwavering guidance, expert advice, and encouragement throughout the conception and execution of this thesis.

I am also profoundly grateful to Prof. Emiliano Nelson Gorr for his constant availability, insightful feedback, and thoughtful suggestions, which have greatly enriched the quality of this work.

I would like to thank my colleague Youssef Sdiri for his generous help, for sharing his expertise, and for contributing part of his work to this project.

I would also like to thank the MORE Center in Torino for providing not only a dedicated workspace but also a truly motivating and supportive community during my time there. Their facilities and collegial atmosphere were instrumental in advancing my research.

Finally, I wish to acknowledge the patience and understanding of my family and friends, whose support kept me motivated throughout this journey. Thank you all for your help, encouragement, and belief in me—this achievement would not have been possible without you.

Table of contents

List of tables VI
List of figures VIII
Acronyms IX
Introduction 1
Technical Foundations of Floating PV Systems 4
2.1 PV module 4
2.2 Tracking Systems 5
2.3 Electrical components 5
2.4 Mooring and anchoring system 6
2.5 Design and classification of the floating structure 6
2.5.1 Pontoon-type 7
2.5.2 Superficial 8
Methodology & Model Framework 10
3.1 Research Workflow 10
3.2 Data Sources 12
3.3 Data Processing & Metrics 12
3.4 FPV Techno-Economic Model 14
3.5 Implementation & Assumptions 14
Results and Discussions 16
4.1 Site Selection Criteria 16
4.2 Platform Class Assignment 22
4.3 Energy Production Analysis 24
4.3.1 Method Overview 24
4.3.2 Solar Resource and Yield Model 25
4.3.3 Annual Energy Output by Site and Class 26
4.3.4 Sensitivity to Performance Parameters. 26
4.4 Detailed Cost Breakdown and Modeling Approach 28
4.4.1 Class 1 28
4.4.2 Class 2 30
4.4.3 Class 3 31
4.4.4 Mooring and anchoring system 33

4.4.5 Electrical components 34
4.5 Energy, Environmental, and Economic Assessment 36
4.5.1 Installation Cost 38
4.5.2 Comparative plots 39
4.5.3 Economies of Scale in CapEx and OpEx Estimation 42
4.6 CO2 Emissions Avoided 43
Summary 46
Interpretation of Class Performance 49
Comparison and Deployment Recommendations 49
Appendices 51
Appendix A – FPV Techno-Economic Model: User Manual 51
Appendix B - Python scripts of the tool 53
Bibliography 57

List of tables

Table 3.1: Summary of data sources, parameters, resolutions, and application in analysis.....12

Table 4.1: Summary of Key Environmental Metrics (2023) with 0.1`box size (11km*11km area centered around the locations) 22

Table 4.2: Platform Class Criteria Based on Environmental Thresholds.....23

Table 4.3: Estimated Annual Energy Output by Platform Class (1 MW System).....26

Table 4.4 shows variations in Module Efficiency.....26

Table 4.5 shows variation in Performance Ratio (PR).....27

Table 4.6: Cost breakdown of Class 1 materials, including unit price, weight, and total cost.....29

Table 4.7: Total cost summary for Class 1 platform, including material and manufacturing costs.....30

Table 4.8: Cost breakdown of Class 2 materials, including unit price, weight, and total cost.....31

Table 4.9: Total cost summary for Class 2 platform, considering materials and increased manufacturing complexity.....31

Table 4.10: Cost breakdown of Class 3 materials, including unit price, weight, and total cost.....32

Table 4.11: Total cost summary for Class 3 platform, considering materials and increased manufacturing complexity due to the modular Hydrelio design.....32

Table 4.12: Summary of the main characteristics of the mooring chain.....33

Table 4.13: Estimated costs for electrical infrastructure components.....34

Table 4.14: Cost breakdown of Class 2 materials, including unit price, weight and total cost.....35

Table 4.15: Input parameters used for the installation cost estimation.....39

Table 4.16: Estimated annual tCO2 emissions avoided by FPV deployment at each location.....44

Table 5.1 Key metrics for 1Mwh.....46

Table 5.2 Key metrics for 10Mwh.....47

Table 5.3 Key metrics for 100Mwh.....47

List of figures

Figure 2.1: Conceptual layout of an FPV installation [2] ……4

Figure 3.1: Research Workflow Flowchart…….....11

Figure 3.2: Example Raw Environmental Data from ERA5 Portal…13

Figure 4.1: Regional Map of Mediterranean Case-Study Site……17

Figure 4.2: Regional Map of North Sea Case-Study Site……...18

Figure 4.3 and 4.4: Histogram of Significant Wave Height….....18

Figure 4.5 and 4.6: Histogram of Wave Energy Period…….....19

Figure 4.7 and 4.8: Monthly Analysis of Significant Wave Height…19

Figure 4.9 and 4.10: Monthly Analysis of Wave Energy Period…….20

Figure 4.11 and 4.12: Yearly Analysis of Significant Wave Height…20

Figure 4.13 and 4.14: Yearly Analysis of Wave Energy Period……..21

Figure 4.15 and 4.16: Joint Occurrence Matrix of Hs and Tp…….22

Figure 4.17: Annual surface solar radiation downward (SSRD) for Site A (Pantelleria) and Site B (North Sea) over the period 2009–2023…24

Figure 4.18: Annual Energy Production Over 20 Years With 2% Degradation…….27

Figure 4.19: Class 1: typical floater design ……29

Figure 4.20: Class 2: floater design from Ciel&Terre [22] ….....30

Figure 4.21: Class 3: floater design from SolarDuck [51]. ……32

Figure 4.22: Cost Breakdown by Platform Class……39

Figure 4.23: Share of cost components for each class. ……..40

Figure 4.24: CapEx sensitivity to Pn. ……41

Figure 4.25: CapEx per MW vs. System Size for both Pantelleria and the North Sea……..42

Figure 4.26 Cumulative tCo2 emissions avoided overtime……45

Figure 5.1 Annual share of exploited vs non-exploited Energy…… 48

Acronyms

BuA Bottom-up Approach
CapEx Capital Expenditure
OpEx Capital Expenditure
DDA Data-Driven Approach
DS Design Structure
AEP annual energy production
Floating Photovoltaics
H_s Significant Wave Height
LCOE Levelized Cost of Energy
NPV Net Present Value
t_{PBT} Payback Time
PV Photovoltaics
RES Renewable Energy Sources
SR Seasonal Removal
TdA Top-down Approach
tCO2 Tons of Carbon Dioxide Equivalent
W Wind speed
u East–west (zonal) component of wind
v North–south (meridional) component of wind
$H_{1/3}$ Average height of the highest one-third of waves
H_j Wave height of the j-th wave
K_t Transmission coefficient
$H_{s,inside}$ Significant wave height inside the protected area
$H_{s,offshore}$ Offshore significant wave height
$x_{99.5}$ 99th percentile value
PVGIS Photovoltaic Geographical Information System
$G_{y,d,h}$ Irradiance value in W/m2 for year y, day d, and hour h
$G_{d,h}$ Mean irradiance at hour h on day d over N years
N Total number of years used for averaging
y Year index
d Day index
h Hour index
G^{daily}_d Total daily irradiance for day d
θ_s Solar elevation angle [°]
ϕ Latitude of the location [°]
δ Solar declination angle [°]
ω Hour angle [°]
β_{opt} Optimal tilt angle [°]
$P_{h,y}$ Power output at hour h of year y
P_h Average power output at hour h over N years
$P_{corr,h}$ Corrected energy production at hour h, accounting for floating cooling effects
γ Correction factor accounting for floating cooling effects
δ Annual degradation rate of the PV system
E_y Annual energy output in year y
$C_{platform}$ Total platform cost

u_i Unit cost of material i
Q_i Quantity of material i
$C_{manufacturing}$ Manufacturing and assembly cost
HDPE High-Density Polyethylene
l_{chain} Length of the mooring chain
H_d Sea depth
C_{chain} Cost of the mooring chain
MBL Minimum Breaking Load
C_{drag} Cost of the drag-embedment anchor
$C_{mooring}$ Total cost of the mooring system
P_n Nominal power of the FPV system [MW]
d_{coast} Distance from the shore [km]
$C_{substation}$ Cost of the electrical substation [€]
C_{cables} Cost of the submarine cables [€]
CPV Total cost of PV modules [€]
P_{panel} Nominal power of a single PV panel [W]
C_{panel} Cost per PV panel [€] xi
AC Alternating Current DC Direct Current
B_t Discounted net cash flow at year t
I Initial investment cost
i Nominal discount rate
MC_t Maintenance cost at year t
C_{kWh} Cost of energy per kilowatt-hour
η_{diesel} Fuel consumption rate of diesel generator [L/kWh]
C_{diesel} Local diesel price [€/L]
C_{grid} Local household electricity price [€/kWh]
Cdiesel-kWh Cost per kWh of electricity generated by diesel
n_{FPV} Total number of floating PV units to be installed
$n_{FPV\_pertrip}$ Number of FPV units transported and deployed per trip
T_{instal}l Installation time per FPV unit
d(x, y) Distance from installation site to shore based on spatial coordinates
v_{boat} Speed of jack-up vessel during transport and installation
C_{boat} Charter cost of jack-up vessel (daily/hourly)
C_{divers} Cost of divers (per unit of time)
$C_{workers}$ Cost of workers (per unit of time)
EF_{avg} Average emission factor [kgCO2/MWh]
E-Diesel Emission factor of the diesel generator [kgCO2/MWh]
EF_{grid} Emission factor of the grid [kgCO2/MWh

Chapter 1
Introduction

Floating photovoltaic (FPV) systems—where PV modules are mounted on rafts or pontoons on water bodies—offer a compelling solution to land-use constraints faced by conventional ground-mounted solar installations. By leveraging unused surfaces on reservoirs, lakes, and coastal zones, FPV can simultaneously reduce evaporation losses, improve module cooling through direct water contact (enhancing yield), and avoid competition with agriculture or urban development. To date, most deployments have been inland, benefiting from calmer waters and existing hydropower infrastructure; offshore applications remain nascent, however, due to harsher wave and wind regimes, higher mooring and installation costs, and limited design guidance for robust open-water platforms.

A critical research gap exists in quantifying how site-specific environmental parameters—significant wave height (Hs), peak wave period (Tp), wind speed, and water depth—influence both the structural design and the overall economics of FPV projects. Top-down studies suggest FPV capex can be 30–40 % higher than equivalent ground-mounted PV, but detailed bottom-up cost breakdowns—especially contrasting offshore pontoons vs. modular float and HDPE-pipe raft solutions—are scarce. Moreover, most techno-economic analyses assume a single fixed plant size and ignore the effects of economies of scale and platform-class–dependent performance.

This thesis develops a dynamic, data-driven FPV model that integrates high-resolution ERA5 and CMEMS reanalysis data with class-specific yield and cost parameters for three platform types. We apply this framework to two representative sites—a Mediterranean location characterized by low Hs and high irradiance, and a North Sea site with high wave energy and moderate solar resources—to compare capex, operational expenditures (OPEX), levelized cost of energy (LCOE), net present value (NPV), and payback time across capacities ranging from X to Y MW. An embedded scoring system—based on Hs, Tp, wind speed, and depth—automatically assigns the optimal platform class to each site, balancing structural resilience with economic efficiency.

By combining bottom-up cost analysis, economies-of-scale modeling, and environmental scoring, this work delivers a robust decision-support tool for rapid site screening and optimization of offshore FPV projects. The insights will inform deployment strategies

and investment decisions, helping to unlock the untapped potential of floating solar in coastal and offshore settings.

Chapter 2: Technical Foundations of Floating PV Systems

Covers the structural and functional components of FPV systems, including PV modules, tracking systems, electrical balance of system (BOS), mooring setups, and platform classifications. Three main platform classes (HDPE-pipe rafts, modular floats, and pontoons) are discussed along with superficial designs, including rigid and flexible variants suited to specific marine environments.

Chapter 3: Methodology & Model Framework

Details the step-by-step modeling framework built using Python. It includes data acquisition (ERA5 and CMEMS), technical sizing, and economic calculations such as CAPEX, OPEX, LCOE, and NPV. Environmental scoring is integrated to assign platform classes automatically. Assumptions and limitations are acknowledged, with emphasis on using a bottom-up approach.

Chapter 4: Case-Study Site Characterization & Environmental Assessment

Describes selection and environmental profiling of two sites: Pantelleria in the Mediterranean and a North Sea location. Wave height, solar radiation, wind speed, and bathymetry are analyzed to guide platform suitability. Environmental metrics are used to classify which FPV type is structurally viable at each site.

Chapter 5: Energy Production Analysis

Presents the model for calculating annual energy output, factoring in solar irradiance, degradation, and platform-specific yield modifiers.

Chapter 6: Detailed Cost Breakdown and Modeling Approach

Breaks down CAPEX for each platform class using a bottom-up method. Material choices, weight, and manufacturing complexity are quantified. Electrical and mooring costs are also included. Class 2 is the most cost-effective but structurally less robust, while Class 3 is the most expensive but offers superior durability.

Chapter 7: Energy, Environmental, and Economic Assessment

Analyzes economic performance via NPV, payback time, and LCOE for various system sizes. Hybrid grid-diesel pricing is used for realistic cost offsets. Larger systems (>10 MW) show significant gains from economies of scale. Pantelleria proves more economically viable than the North Sea at smaller scales.

Chapter8: Results and Discussions

Synthesizes results across all classes and sites. Class 1 yields fastest payback and best LCOE, especially in the Mediterranean. Class 3 is favored for harsher environments. Economic feasibility improves dramatically with scale. Pantelleria outperforms the North Sea under current assumptions, particularly in carbon offset and return on investment.

Summary

This thesis highlights the strong potential of Floating Photovoltaic (FPV) systems in both calm and challenging marine environments.

By combining detailed environmental data and cost modeling, three FPV platform types were evaluated at sites in the Mediterranean and North Sea. Results showed:

- Small-scale FPV (1 MW) is only viable in favorable conditions like Pantelleria.
- Larger systems (10–100 MW) are viable even in rougher environments due to economies of scale.
- Class 1 platforms offered the best economic performance, Class 3 delivered the highest yields, and Class 2 provided a balanced option.

Future Outlook

Offshore FPV promises large-scale clean energy due to:

- Low land use and synergy with other coastal systems
- Opportunities for design innovation, digital monitoring, and hybrid systems
- Policy support as a key driver for wider adoption

FPV is poised to become a key solution for sustainable offshore energy development.

Appendix A

User manual for the Python tool

Appendix B

Python code with important functions

Bibliography

References and sources used

Chapter 2.

Technical Foundations of Floating PV Systems

A typical FPV installation consists of photovoltaic modules for energy capture, buoyant floating platforms, a support frame for the panels, a mooring arrangement to prevent drift, and the necessary electrical balance-of-system components to connect into the grid. As shown in Fig. 2.1, FPV systems operate on the same basic principles as land-based PV arrays; the only fundamental distinction is that the solar panels are affixed to a floating structure rather than fixed to the ground.

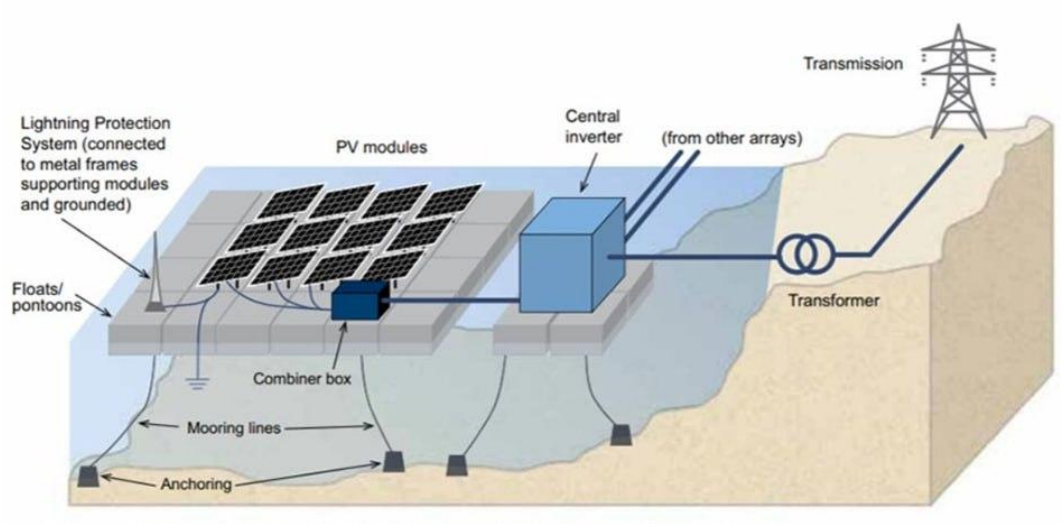

Figure 2.1: Conceptual layout of an FPV installation [2]

2.1 PV module

Floating PV installations employ the same module technology as land-based systems: solar cells made from light-absorbing semiconductors that capture photons and generate electricity via the photovoltaic effect. Although commercial FPV arrays typically use standard crystalline-silicon modules, experimental thin-film panels—valued for their flexibility under wave loading—are under investigation but not yet widely deployed. In a marine setting, modules must also endure higher mechanical stresses and resist saltwater corrosion, which accelerates degradation and exacerbates soiling losses from dust, bird droppings, and airborne particles.

Surface fouling can create shaded “hot spots” that permanently damage cells, so we account for an annual performance decline of 2 % to capture degradation effects. Bifacial modules, which harvest light from both faces by exploiting ground-reflected albedo, offer up to a 13.5 % yield increase when paired with reflective float surfaces, although their benefit over water—naturally low in albedo—is limited without added reflectors.

2.2 Tracking Systems

Tracking mechanisms can significantly boost FPV output by allowing the PV modules to follow the sun’s path. Both single-axis (horizontal or vertical) and dual-axis trackers are possible: a vertical-axis tracker might use a submerged rotating platform that turns the entire floating array, whereas a horizontal-axis tracker simply mounts the panel frame on an adjustable-tilt structure. Whether a given tracking solution is feasible depends on the pontoon design—some float types only support fixed, flat panels with no tilt adjustment. Dual-axis trackers can raise energy yield by up to 30 %, but they also nearly double system costs

2.3 Electrical components

Power generated by the FPV array must be collected and converted before feeding into the grid, requiring a network of underwater or overhead cables and electrical balance-of-system components. All cables, whether buried beneath the water or suspended above—must be fully waterproof and specified to withstand intense UV exposure and wide temperature swings. Because solar output is intermittent, DC–DC converters are used to step up the array’s voltage, followed by an inverter to transform DC into grid-compatible AC.

These power-electronics can be housed either onshore or directly on the floating platform. In an onshore substation configuration, the export cable from the FPV system carries DC to land, where all voltage conversion and inversion occur before connection to the transmission network. Alternatively, if the converters and inverters are mounted on the floats, the export cable carries AC directly to the grid. Whenever feasible, locating the substation onshore is preferred—installation is simpler, maintenance costs are lower, and critical equipment remains accessible without marine-environment service challenges.

2.4 Mooring and anchoring system

The mooring system is critical for keeping the floating platform securely in place against wind, waves, and currents, thereby preventing collisions or structural damage. In offshore FPV installations, mooring lines are usually made of steel chains and anchors often consist of driven concrete piles. Mooring arrangements generally fall into four categories:

- Catenary mooring: Relies on heavy chain weight to create a natural, curved profile that provides both flexibility and restoring force to stabilize the platform.

- Compliant mooring: Builds on the catenary approach by adding floats or weights along the lines to tune their stiffness and dynamic response.

- Taut mooring: Keeps the lines under constant high tension, often using additional buoyancy elements, resulting in minimal platform displacement.

- Rigid mooring: Uses fixed structural members anchored directly to the seabed; it allows vertical movement with waves but constrains horizontal drift and sway.

2.5 Design and classification of the floating structure

In recent years, a wide variety of floating photovoltaic platforms have emerged, tailored to local conditions through different materials and designs. The DNV Recommended Practice DNVGL-RP-0584 defines three primary FPV configurations:

- Pure float systems: PV modules are secured directly onto individual floats using integrated clamps or fixtures. Each float is engineered to carry one or more modules.
- Membrane-based systems: Solar panels rest on a reinforced, buoyant membrane that is supported by tubular rings or similar structures, which also house auxiliary equipment like combiner boxes.

• Taut-mooring systems: Lines remain in constant tension—often aided by extra buoyancy elements—to minimize platform movement.

• Rigid-mooring systems: Structural members are fixed firmly to the seabed, permitting only vertical heave while preventing horizontal drift and sway.

An alternate, widely cited classification group FPV by how the panels relate to the water surface. “Superficial” arrays mount modules directly at the waterline, benefiting from enhanced natural cooling but facing greater wave-induced stress. In contrast, “pontoon-type” systems elevate the panels on a floating deck or platform, providing more robust protection while still leveraging water cooling effects.

2.5.1 Pontoon-type

The main characteristic of the pontoon type is the presence of a raft to give stability to the solar modules, and there are three different main classes based on the different existing design.

Class 1

Class 1 FPV platforms represent the original floating designs, featuring rafts composed of parallel HDPE cylinders topped with steel, aluminum, or fiber-reinforced–plastic support structures. With minimal water contact, these systems readily integrate features such as single-axis trackers but incur higher costs than other classes. The world’s first large-scale, commercial FPV installation—a 200 kW freshwater array in Suvareto, Italy—used this Class 1 configuration. In marine settings, Class 1 arrays have performed well under moderate wave conditions, though they can experience excessive flexural stresses. To mitigate this, hinged connections or alternative floater geometries are sometimes employed. For example, the Swimsol SolarSea system replaces cylindrical floats with aligned pontoons and mounts the panels on an elevated aluminum truss to minimize saltwater exposure.

Class 2

Class 2 FPV platforms, first commercialized by Ciel & Terre in 2011 under the Hydrelio brand, mount each solar panel on an individual float equipped with integrated rails. These floats can incorporate electrical housing, function as perimeter barriers, or even serve as walkways. Adjacent floats snap together via pins, eliminating the need for a separate supporting superstructure. As a result, Class 2 systems are more cost-effective than Class 1 designs, though their

modular rail-based layout limits customization—such as adding tracking or other efficiency upgrades.

With greater surface contact with water, Class 2 floats are more prone to material wear and environmental stress, and while they typically perform well in freshwater at wave heights up to 1 m, they are less suited to open-sea conditions. Nevertheless, their affordability has driven widespread adoption: for example, a sheltered nearshore installation in the Persian Gulf employed bifacial panels to resist salt spray, and Chenya Energy's Hydrelio array off Taiwan briefly held the title of world's largest offshore solar plant. Despite these successes, fully offshore deployments continue to pose durability and performance challenges for this class.

Class 3

Class 3 FPV platforms are built by connecting individual floats into a single, walkable "island" on which solar panels and electrical equipment are mounted independently. Their rigid deck eliminates the need for narrow catwalks, resulting in a highly stable, safe structure that simplifies maintenance—albeit at a higher cost than other designs. Variations include replacing HDPE floats with concrete pontoons for even greater durability. Because of their robust construction, Class 3 systems excel in harsh marine conditions; for example, Oceans of Energy's Dutch North Sea installation—the world's first "high-wave" FPV—has withstood storms with wave heights up to 10 m.

2.5.2 Superficial

This category has the characteristics of having a thin layer of water covering the PV modules: this has the advantage of increasing the cooling effect and mitigates the effect of wind loads on the modules, while on the other hand we have direct loads from the waves and the increase of corrosion due to the salinity of the sea water. In two different strategies have been proposed to withstand these environmental conditions: the rigid and the flexible approach.

Rigid

A rigid FPV plant has been proposed by, and it's said that can submerge up to 2 meters and to be able to withstand the waves loads, this is since the wave induced velocity of water it decrease with water depth. But the light that can reach the modules will be much lower, due to the light absorbed by the water, with the consequence of reduced energy production by the system.

Flexible

The flexible FPV strategy includes two main approaches: Thin-film flexible mod- ules, typically made from amorphous silicon, and the crystalline silicon modules supported with flexible foam. Thin-film modules are lightweight, use minimal materials, and offer advantages like natural cooling, fewer components, better wave resistance, and lower mooring system costs due to reduced hydrodynamic interaction. However, they cannot be tilted or tracked, and wave motion may affect module orientation, lowering efficiency compared to pontoon-based systems. Even if they are not submerged, the closest distance from the water enhances cooling, potentially increasing yield by 5% over pontoon systems. Ocean Sun is testing systems in the Canary Islands and South Korea. A Dutch company is also test in a 20-kW pilot system in the Port of Rotterdam, aiming to scale it up to 5 MW on the North Sea.

Chapter 3.

Methodology & Model Framework

3.1 Research Workflow

The research workflow employed in this thesis follows a structured, systematic approach designed to evaluate the techno-economic viability of floating photovoltaic (FPV) systems. This workflow encompasses multiple integrated steps:

1. Definition of Input:
    - Selection of geographic coordinates (latitude and longitude).
    - Specification of analysis parameters, including year, desired system capacity, and platform class.
2. Environmental Data Retrieval:
    - Utilization of ERA5 and CMEMS datasets to obtain site-specific environmental data, including solar radiation (SSRD), wave characteristics (Hs, Tp), wind speed components (u10, v10), and bathymetric data.
    - Extraction and analysis of logistical data, particularly distances to the nearest ports from the deployment sites.
3. Metric Computation:
    - Processing and summarizing data into meaningful annual metrics (e.g., mean wave height, mean wind speed, total annual solar irradiance).
    - Calculation of derived metrics such as the energy production potential in MWh per MW installed.
4. Technical Sizing:
    - Determination of FPV system dimensions, including module counts, array area, and the selection of appropriate structural and mooring designs based on environmental scoring.
5. Economic and Financial Assessment:

- Bottom-up estimation of capital expenditures (CapEx) and operational expenditures (OpEx), factoring in economies of scale.

- Calculation of key financial indicators, including Net Present Value (NPV), payback time, and Levelized Cost of Energy (LCOE).

6. Integration and Analysis:

   - Synthesizing environmental, technical, and economic data into a comprehensive analysis for decision-making support.

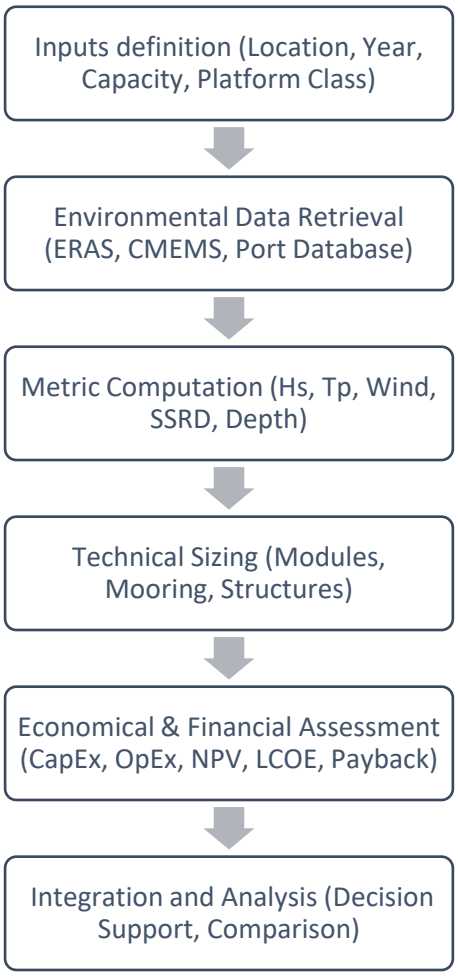

Figure 3.1: Research Workflow Flowchart

The above workflow provides a robust framework to systematically compare FPV projects across diverse geographic and environmental conditions.

3.2 Data Sources

The primary data sources utilized in this study include:

ERA5 Reanalysis Dataset: Provided by ECMWF, this dataset supplies meteorological parameters, including solar radiation (SSRD), wind components (u10, v10), and bathymetric data.

Copernicus Marine Environment Monitoring Service (CMEMS): Supplies high-resolution wave data, specifically significant wave height (Hs) and peak wave period (Tp).

Port Data: Geographic information extracted from a comprehensive port database (CSV format), which includes locations and related logistical details critical for site accessibility assessments.

Table 3.1: Summary of data sources, parameters, resolutions, and application in analysis.

Data Source	**Parameters**	**Spatial Resolution**	**Temporal Resolution**	**Application**
ERAS	SSRD, wind speed, bathymetry, Hs	0.1°	Hourly/ Daily	Environmental Analysis, Energy yield
CMEMS	Tp	0.2°	Hourly	Wave climate characterization
Port Database	Port locations, distances	Point data	Static	Logistical cost estimation

3.3 Data Processing & Metrics

Environmental and logistical data retrieved from various sources undergo standardized processing to yield meaningful and comparable metrics:

Wave Climate Metrics: Calculation of annual mean significant wave height (Hs) and peak period (Tp), including percentile analysis to characterize extreme events.

$$Hs_{mean} = \frac{1}{N}\sum_{i=1}^{N} Hs_i \qquad (3.1)$$

$$Tp_{mean} = \frac{1}{N}\sum_{i=1}^{N} Tp_i \qquad (3.2)$$

Wind Regime Metrics: Derivation of average annual wind speed through vector calculations based on u10 and v10 wind components.

$$W_{mean} = \frac{1}{N}\sum_{i=1}^{N}\sqrt{u10_i^2 + v10_i^2} \qquad (3.3)$$

Solar Resource Metrics: Computation of total annual surface solar radiation downward (SSRD), subsequently converted to energy yield (MWh/MW/year).

Bathymetric Metrics: Determination of average water depth within the defined spatial boundaries for site assessment.

$$Depth_{mean} = \frac{1}{N}\sum_{i=1}^{N} Depth_i \qquad (3.4)$$

Logistics Metrics: Identification of the nearest port and calculation of geodesic distance to quantify potential logistical impacts on project feasibility.

These computed metrics form a crucial basis for subsequent technical and economic evaluations.

format	netcdf
Product type	Monthly averaged reanalysis
Variable	Surface solar radiation downwards
Year	2022
Month	January, February, March, April, May, June, July, August, September, October, November, December
Time	00:00
Geographical area	North: 36.873°, West: 11.270299999999999°, South: 36.773°, East: 11.3703°
Data format	GRIB
Download format	Unarchived (not zipped if single file)

Figure 3.2: Example Raw Environmental Data from ERA5 Portal (https://cds.climate.copernicus.eu)

3.4 FPV Techno-Economic Model

The FPV techno-economic model developed in this study integrates multiple components and processes to assess the viability and performance of floating photovoltaic systems comprehensively. The model includes:

Technical Sizing: Calculation of FPV system size, including the determination of the required number of photovoltaic modules, platform size, and mooring components based on environmental metrics and targeted power generation.

Capital Expenditure (CapEx) Estimation: Detailed breakdown of initial investment costs, covering modules, floating structures, anchoring and mooring systems, electrical infrastructure, and installation activities.

Operational Expenditure (OpEx) Estimation: Evaluation of recurring maintenance, operational management, and logistical support expenses over the project lifespan.

Economies of Scale: Integration of scaling factors to reflect cost efficiencies realized with increasing project size.

Financial Metrics: Calculation of economic performance indicators, including Net Present Value (NPV), Payback Period, and Levelized Cost of Energy (LCOE), to facilitate investment decisions.

3.5 Implementation & Assumptions

The FPV techno-economic model was implemented using Python programming language, employing various scientific libraries such as cdsapi, xarray, pandas, geopandas, and NumPy to ensure efficient data handling and processing. Key assumptions made during model development include:

A constant discount rate of 6% for financial evaluations.

Fixed photovoltaic module efficiency and performance ratio.

Utilization of fixed-depth and fixed-distance assumptions where detailed measurements are unavailable.

Limitations inherent to the model include uncertainties associated with the reanalysis data sources, potential variability in real-world logistical constraints, and assumptions of stable economic factors over the project's lifetime.

Chapter 4

Results and Discussions

4.1 Site Selection Criteria

The selection of case-study sites in this thesis is guided by the need to assess floating photovoltaic (FPV) feasibility across distinct marine environments. The goal is to evaluate how environmental variability—especially in wave energy, irradiance, and bathymetry—affects platform choice, energy yield, and cost-efficiency.

The two selected sites reflect contrasting but realistic deployment scenarios:

Site A: A sheltered Mediterranean location with high solar radiation and low wave activity, typical of southern Europe's coastal energy profile.

Site B: A North Sea location characterized by higher wave energy, moderate irradiance, and more demanding structural conditions.

Key selection criteria include:

Wave regime: Differentiated significant wave height (Hs) and peak wave period (Tp)

Solar potential: High vs. moderate SSRD (surface solar radiation downwards)

Wind speed: Representative average marine wind speeds

Water depth: Feasible mooring depths (15–25 m range)

Port access: Proximity to coastal infrastructure to support installation and maintenance

Data availability: Full-year environmental data from ERA5, CMEMS, and Polito datasets

By contrasting these sites, the analysis reveals how FPV performance and costs scale under varied marine forcing, guiding location-specific technology choice and financial planning.

The two geographic points selected for this analysis are:

Site A: Mediterranean Sea – Pantelleria, Italy

Coordinates: 36.823° N, 11.3203° E

Located between Sicily and Tunisia, Pantelleria lies in a solar-rich region with moderate wind and very low wave activity. The site benefits from relative shelter, low turbidity, and proximity to small harbor infrastructure. These factors make it a strong candidate for Class 1 or Class 2 floating platforms.

Site B: North Sea – West Frisian Islands, The Netherlands

Coordinates: 53.42° N, 5.6° W

This open-water site lies offshore of the Dutch coast, exposed to frequent Atlantic weather systems. It experiences strong winds and higher wave energy compared to the Mediterranean, making it representative of challenging North Sea conditions. The proximity to Dutch ports supports offshore logistics but necessitates more robust platform solutions such as Class 3.

These sites were selected not only for their geographic contrast but also for their relevance to ongoing marine energy research and data accessibility.

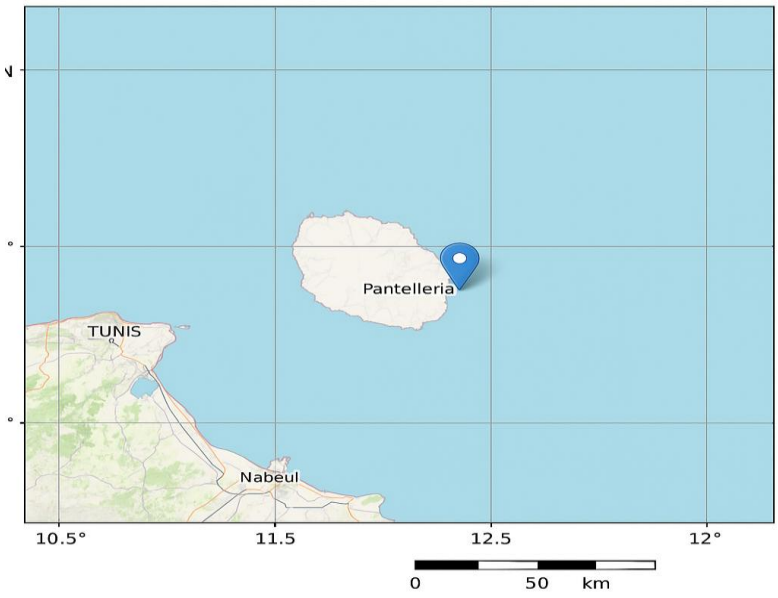

Figure 4.1: Regional Map of Mediterranean Case-Study Site

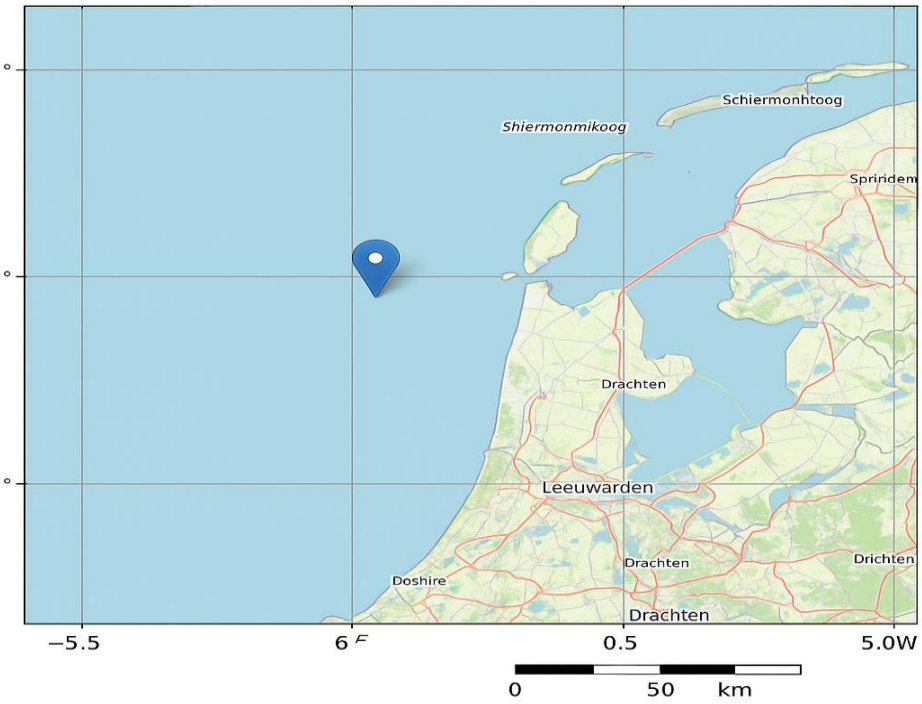

Figure 4.2: Regional Map of North Sea Case-Study Site

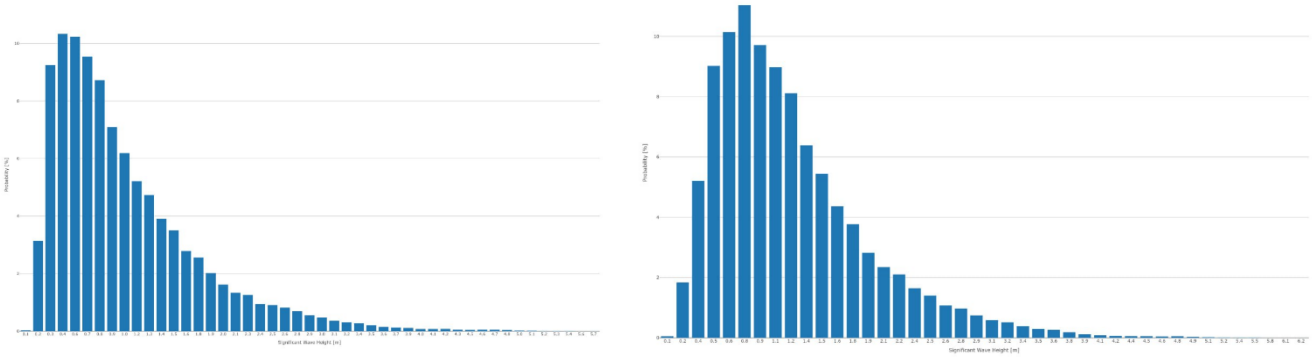

Figure 4.3 and 4.4: Histogram of Significant Wave Height (wave.est.polito.it)

Figure 4.3: Probability distribution of significant wave height (Hs) at Site A (Pantelleria) over a 12-month period. Most Hs values fall below 1.5 meters, with over 60% of observations below 1.0 m, indicating predominantly calm sea states favorable for Class 1 or 2 floating platforms.

Figure 4.4: Probability distribution of significant wave height (Hs) at Site B (North Sea). The distribution is broader than at Site A, with a peak around 0.8–1.0 m and a longer tail extending beyond 5.0 m, indicating the presence of more frequent and higher-energy wave events.

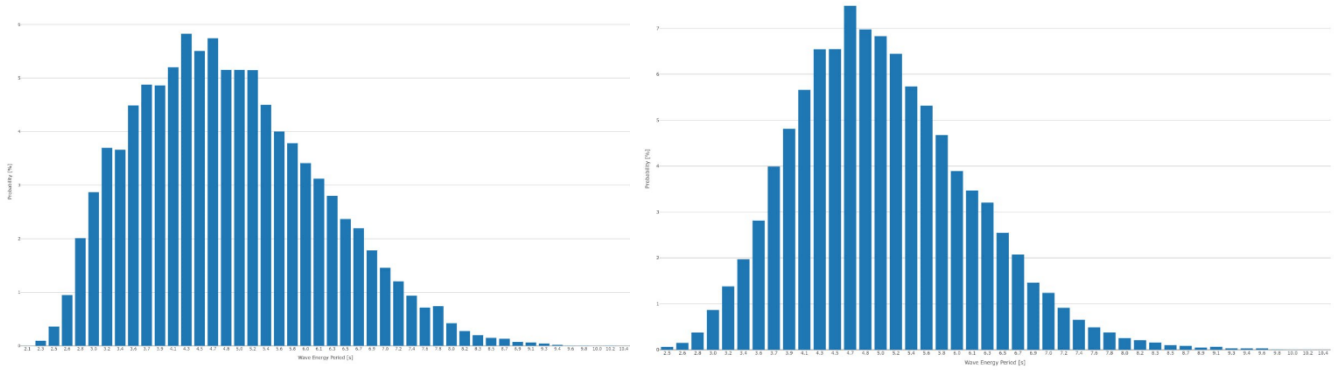

Figure 4.5 and 4.6: Histogram of Wave Energy Period (wave.est.polito.it)

Figure 4.5: Probability distribution of wave energy period (Tp) at Site A (Pantelleria). Most wave periods fall between 3.5 and 6.5 seconds, peaking around 4.5–5.0 seconds. These short-period swells indicate relatively benign wave forcing, favorable for lighter mooring and platform configurations.

Figure 4.6: Probability distribution of wave energy period (Tp) at Site B (North Sea). The distribution peaks around 4.5 to 5.0 seconds, with a broad tail extending beyond 8.0 s. This indicates the presence of longer-period waves compared to Site A, consistent with deeper water and higher fetch exposure.

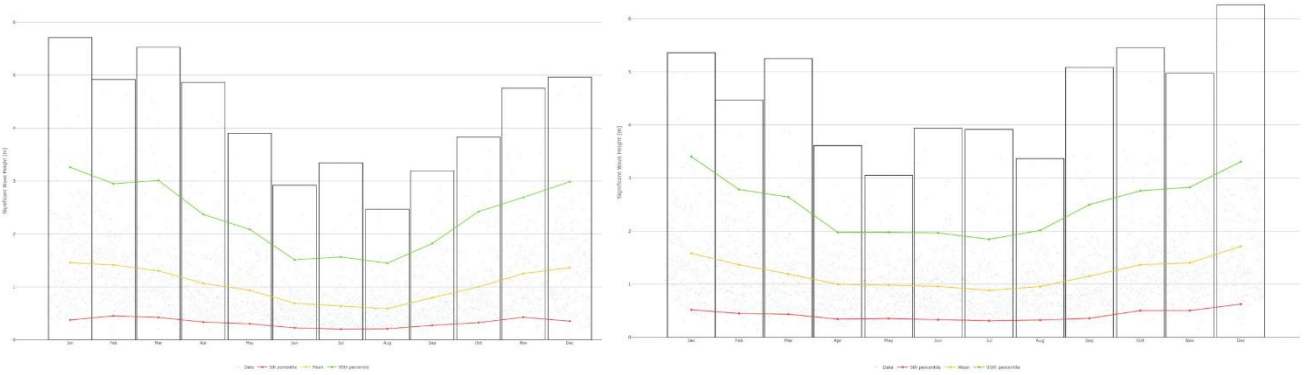

Figure 4.7 and 4.8: Monthly Analysis of Significant Wave Height (wave.est.polito.it)

Figure 4.7: Monthly variation in significant wave height (Hs) at Site A (Pantelleria), showing 5th percentile (red), mean (yellow), and 95th percentile (green) values. The summer months (June–August) exhibit the calmest conditions, while winter months (December–

February) see increased wave heights, reaching up to 3.2 m at the 95th percentile.

Figure 4.8: Monthly variation in significant wave height (Hs) at Site B (North Sea). Winter months (Dec–Feb) show higher mean and 95th percentile values, with peak events exceeding 3.0 m. Summer months (Jun–Aug) exhibit calmer conditions, though still more energetic than Site A.

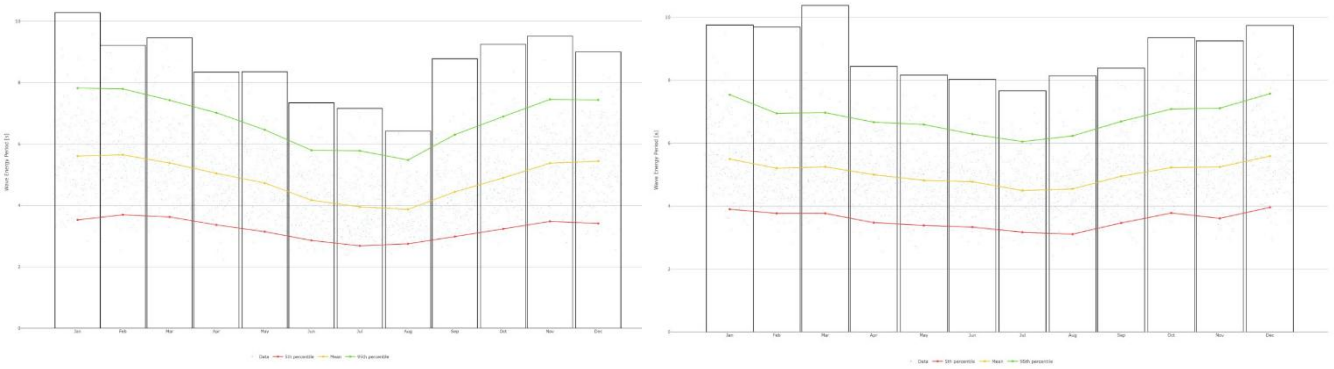

Figure 4.9 and 4.10: Monthly Analysis of Wave Energy Period (wave.est.polito.it)

Figure 4.9: Monthly variation in wave energy period (Tp) at Site A (Pantelleria), displaying 5th percentile (red), mean (yellow), and 95th percentile (green) values. Tp values are shortest during summer months (June–August) and longest in winter (November–January), following the seasonal wave energy trend in the Mediterranean.

Figure 4.10: Monthly variation in wave energy period (Tp) at Site B (North Sea). Mean values remain above 5.0 s year-round, with 95th percentiles reaching 7.5–8.0 s during the winter season. These longer periods reflect high-energy swells, underscoring the need for structurally resilient FPV platforms.

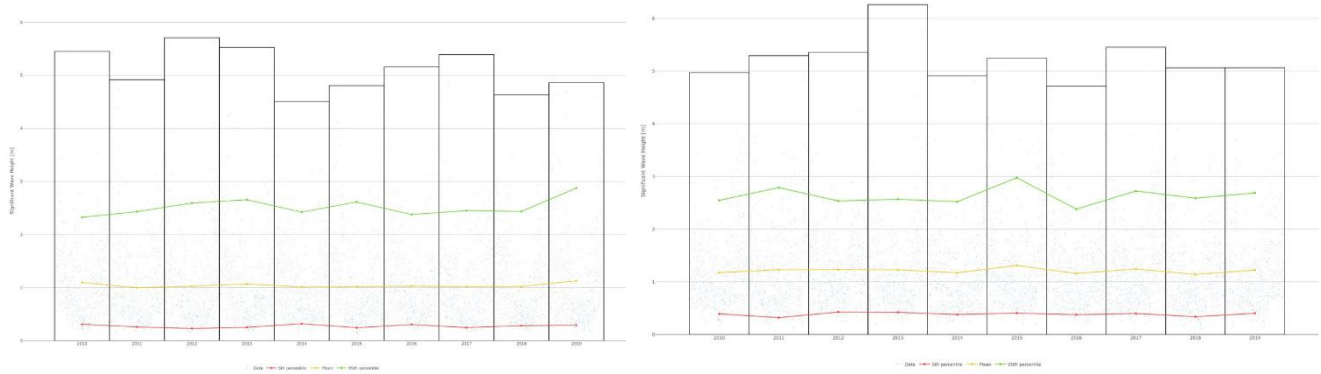

Figure 4.11 and 4.12: Yearly Analysis of Significant Wave Height (wave.est.polito.it)

Figure 4.11: Annual variation in significant wave height (Hs) at Site A (Pantelleria) from 2010 to 2019. While year-to-year variability is modest, the mean remains relatively stable (~1.0 m), with 95th percentile values fluctuating between 2.4 and 2.9 m, confirming long-term suitability for FPV deployment in a low-wave regime.

Figure 4.12: Yearly variation in significant wave height (Hs) at Site B (North Sea) from 2010 to 2019. The mean Hs remains stable around 1.1–1.2 m, while 95th percentile values consistently range from 2.4 to 3.0 m, reflecting a persistent high-energy environment over the decade.

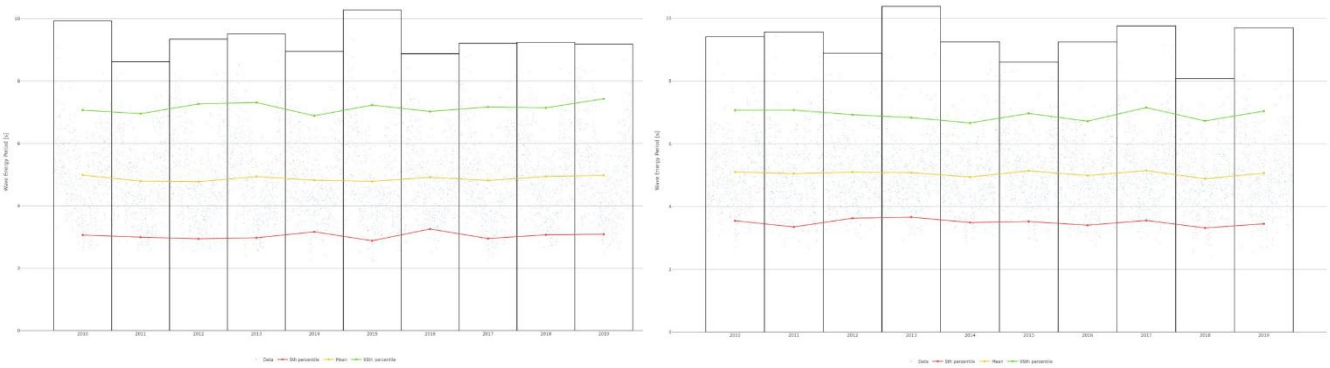

Figure 4.13 and 4.14: Yearly Analysis of Wave Energy Period (wave.est.polito.it)

Figure 4.13: Yearly variation in wave energy period (Tp) at Site A (Pantelleria) from 2010 to 2019. The mean Tp remains consistent (~5.0 s), with 95th percentile values ranging from 6.8 to 7.5 seconds. The limited variability further supports stable long-term design assumptions for platform classification and mooring design.

Figure 4.14: Yearly variation in wave energy period (Tp) at Site B (North Sea) from 2010 to 2019. Mean Tp remains steady around 5.2–5.4 seconds, with 95th percentile values consistently between 6.8 and 7.3 seconds. This indicates persistent long-period swell conditions, supporting the need for robust platform anchoring systems.

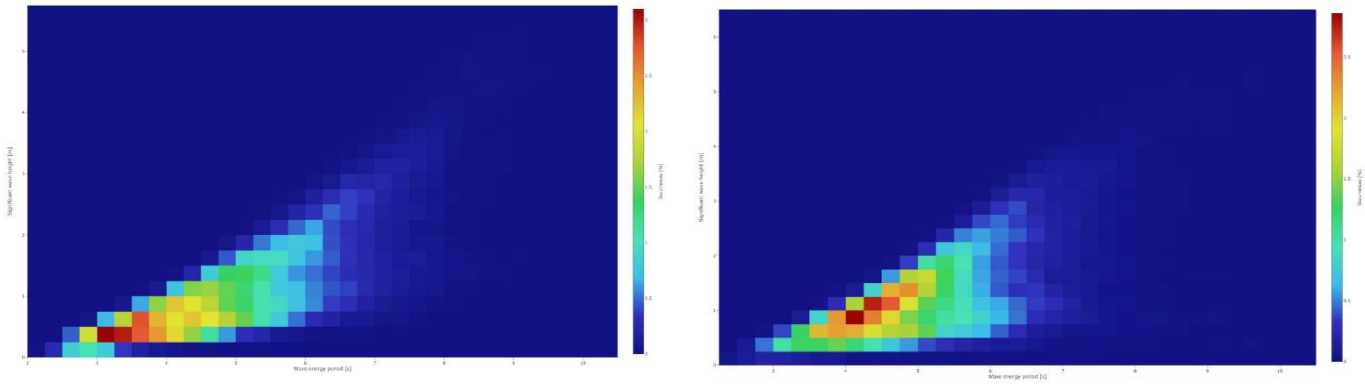

Figure 4.15 and 4.16: Joint Occurrence Matrix of Hs and Tp (wave.est.polito.it)

Figure 4.15: Joint occurrence matrix of significant wave height (Hs) and wave energy period (Tp) at Site A (Pantelleria). Most wave events cluster below 1.5 m in Hs and between 3–6 s in Tp, confirming the low-energy sea state. This reinforces the suitability of lightweight mooring and Class 1–2 floating structures.

Figure 4.16: Joint occurrence matrix of significant wave height (Hs) and wave energy period (Tp) at Site B (North Sea). The most frequent sea states occur between 0.9–1.5 m in Hs and 4.0–6.0 s in Tp, indicating frequent exposure to mid-energy waves typical of shallow shelf seas.

Table 4.1: Summary of Key Environmental Metrics (2023) with 0.1`box size (11km*11km area centered around the locations)

Parameter	**Site A**	**Site B**
Mean Hs (m)	0.86	1.26
Mean Tp (s)	4.28	8.15
Mean Wind Speed (m/s)	5.50	7.16
Depth (m)	191	24
Closest Port	Tazerka Oil Terminal	Harlingen
Distance to Port (km)	40.8	29

4.2 Platform Class Assignment

Platform class assignment is based on key environmental parameters, including significant wave height (Hs), wave energy period (Tp), and wind speed. These variables are compared against

refined thresholds derived from design criteria and classification studies.

Table 4.2: Platform Class Criteria Based on Environmental Thresholds

Parameter	**Class 2**	**Class 1**	**Class 3**
Hs (m)	$Hs < 1.47$	$1.47 \leq Hs < 2.08$	$2.08 \leq Hs \leq 4.03$
Tp (s)	$Tp < 5.5$	$5.5 \leq Tp < 7.0$	$Tp \geq 7.0$
Wind Speed (m/s)	$WS < 6.0$	$6.0 \leq WS < 8.0$	$WS \geq 8.0$

4.3 Energy Production Analysis

4.3.1 Method Overview

This chapter presents the methodology and results of the energy production analysis for floating photovoltaic (FPV) systems at the two selected case-study sites. The objective is to estimate the annual electricity yield in megawatt-hours (MWh) based on site-specific solar irradiance and system characteristics, while accounting for platform class variations.

The primary environmental input for energy production is the annual surface solar radiation downward (SSRD), sourced from the ERA5 reanalysis dataset. SSRD values are extracted for each site's bounding box and summed over the calendar year to obtain the total incoming solar energy in joules per square meter. These values are converted to kilowatt-hours per square meter (kWh/m²) using the standard factor:

$$SSRD_{kWh/m^2} = \frac{SSRD_{J/m^2}}{3.6 \times 10^6} \qquad (4.1)$$

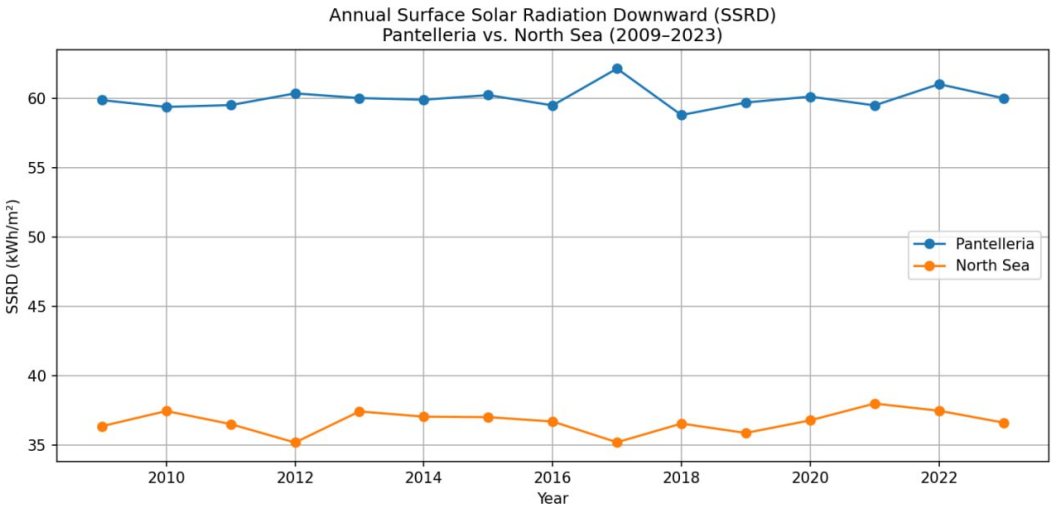

Figure 4.17: Annual surface solar radiation downward (SSRD) for Site A (Pantelleria) and Site B (North Sea) over the period 2009–2023. Pantelleria shows

consistently higher irradiance with low interannual variability, whereas the North Sea exhibits moderately lower and more variable solar availability

4.3.2 Solar Resource and Yield Model

The net energy output of the FPV system is calculated using the following formula:

$$Annual\ Energy\ Output = SSRD_{kWh/m^2} \times \eta_{STC} \times PR \times A \times EF \quad (4.2)$$

Where:
η_{STC} is the module efficiency under standard test condition (assumed 20%)
PR is the performance ratio accounting for system losses (assumed 80%)
A is the active module required to achieve the system capacity
EF is the energy factor, which adjusts output based on FPV platform class
Active area A is calculated as:

$$A = \frac{Capacity_{MV} \times 10^6}{1000 \times \eta_{STC}} \quad (4.3)$$

Platform class influences energy production through the class-dependent energy factor (EF):

Class 1: EF = 1.00

Class 2: EF = 0.90 (e.g., limited tracking or tilt adjustment)

Class 3: EF = 1.10 (e.g., bifacial modules or active cooling systems)

$$P_{corrected} = \gamma \times P, \quad \gamma = 1.10 \quad (4.4)$$

Finally, to account for annual degradation in energy yield over time (with degradation rate δ = 2%), the yearly production for year y is given by:

$$E_y = E_1 \times (1 - \delta)^{y-1} \quad (4.5)$$

This methodology enables consistent and scalable energy yield estimation across both sides and all platform configurations.

4.3.3 Annual Energy Output by Site and Class

To evaluate the effect of platform design on energy output, the gross annual yield from each site is scaled by the corresponding class-based energy factor (EF). This adjustment accounts for differences in yield-enhancing features such as bifacial modules or tracking systems.

Table 4.3: Estimated Annual Energy Output by Platform Class (1 MW System)

Site	Class 1 (EF = 1.00)	Class 2 (EF = 0.9)	Class 3 (EF = 1.10)
Site A	1,462 MWh	1,316 MWh	1,609 MWh
Site B	928 MWh	835 MWh	1,020MWh

As expected, Site A consistently delivers higher energy output across all platform classes due to its superior solar resource. Class 3 systems offer enhanced yields owing to design improvements, but these must be weighed against higher capital and operational costs in later chapters.

4.3.4 Sensitivity to Performance Parameters.

To assess the robustness of the energy yield model, we analyze its sensitivity to key system parameters, namely:

- Module Efficiency (η_{STC})
- Performance Ratio (PR)
- Degradation Rate (δ)
- Energy Factor (EF)

Variation in Module Efficiency
Assuming the base case $\eta_{STC} = 0.2$, we explore a $\pm 2\%$ range:

Table 4.4 shows variations in Module Efficiency

Efficiency	Site A Output (MWh)	Site B Output (MWh)
0.18	1,316	835
0.2	1,462	928
0.22	1,609	1,020

A change in PR from 0.75 to 0.85 shows:

Table 4.5 shows variation in Performance Ratio (PR)

PR value	Site A Output (MWh)	Site B Output (MWh)
0.75	1,371	870
0.8	1,462	928
0.85	1,553	986

Degradation Over Time
Considering a 2% annual degradation:

$$E_y = E_1 \times (1 - 0.02)^{y-1} \quad (4.6)$$

This results in approximately 32% cumulative energy loss over 25 years. Class 3 systems, with higher initial production, may preserve more long-term value despite a slightly steeper decline. These sensitivities emphasize the importance of site-specific calibration and class-appropriate performance assumptions in techno-economic modeling.

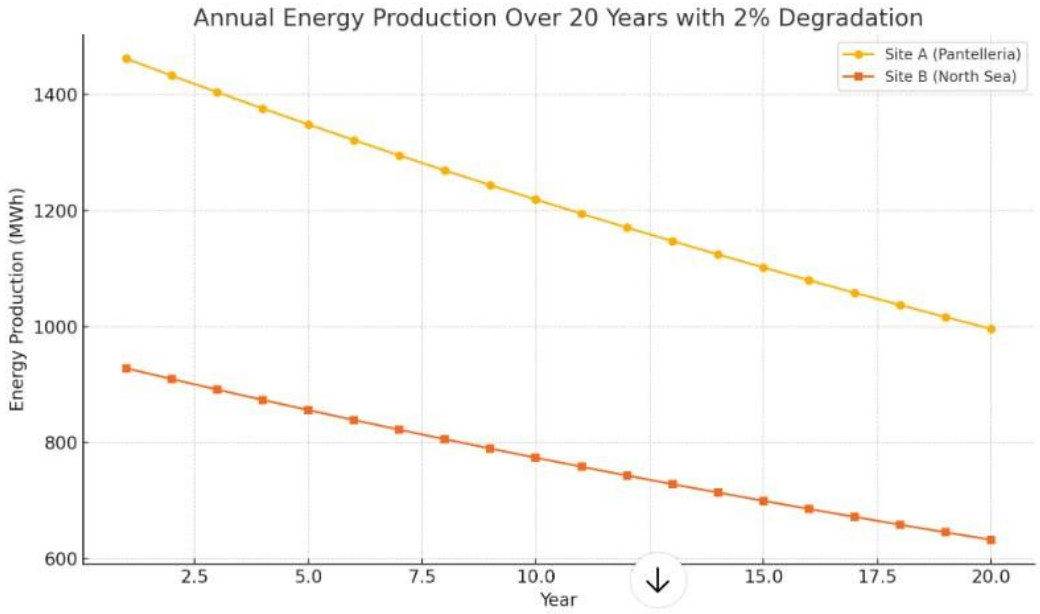

Figure 4.18 Annual Energy Production Over 20 Years With 2% Degradation

4.4 Detailed Cost Breakdown and Modeling Approach

A bottom-up approach (BuA) is utilized to estimate the costs related to various floating platform designs and their associated mooring systems. This method involves breaking down each FPV platform into its essential structural components, characterized by defined material properties and geometric parameters. The cost of each element is then calculated independently, and the overall platform cost is derived by summing the individual component costs [50].

After specifying the geometry and material composition, the total cost of the platform is computed using the following equation:

$$C_{platform} = \sum_i (u_i \times Q_i) + C_{manufacturing} \quad (4.7)$$

Where ui represents the unit cost of material i, and Qi is the corresponding quantity required. The term Cmanufacturing accounts for manufacturing and assembly costs, which are estimated based on the complexity of the structure, including factors such as fabrication processes, required labor, and the level of customization

4.4.1 Class 1

The material composition and structural configuration of the Class 1 floating platform are based on the design presented by Guido et al. in [9]. As it's shown in Fig.6.1 The platform is divided into three main components: the floaters, the module-supporting frame, and the support structure connecting the frame to the floaters. A platform area of 124 m2 is considered, allowing for the installation of approximately 70 photovoltaic modules.

Figure 4.19: Class 1: typical floater design

The materials selected for each component were chosen based on mechanical performance, corrosion resistance, and cost effectiveness for offshore environments.
The Support structure is made of AISI 205 steel, selected for its structural strength and corrosion resistance in saline conditions. While the Frame structure comes from Aluminium 5005, which offers a balance between light weight and high corrosion resistance, suitable for components under lower structural loads, and the floaters are abricated from High-Density Polyethylene (HDPE), chosen for its UV and saltwater resistance, mechanical robustness, and relatively low cost.

Table 4.6: Cost breakdown of Class 1 materials, including unit price, weight, and total cost

Material	Mass	Cost	Total Cost
Aliminium 5005	138.1	2.43	336
Steel AISI 205	2,615.1	3	7,845
HDPE	265.36	1.216	1,291
*	kg	€/kg	€

This structured breakdown enables a detailed and transparent cost estimation, forming the basis for further techno-economic analysis of Class 1 systems. In Table 4.6, the overall cost estimation is completed by including the manufacturing and assembly expenses.

Table 4.7: Total cost summary for Class 1 platform, including material and manufacturing costs

Material/Service	Cost	Unit of Measure
Aliminium 5005	336	€
Steel AISI 205	7,845	€
HDPE	1,291	€
Manufacturing work/assemmbly	1,894	€
Total	11,366	€

4.4.2 Class 2

For the Class 2 system, the design adopted is based on the commercially available. Hydrelio platform developed by Ciel & Terre [22]. This modular system consists of floaters capable of supporting individual photovoltaic panels, with a detailed structural layout illustrated in Fig. 6.2

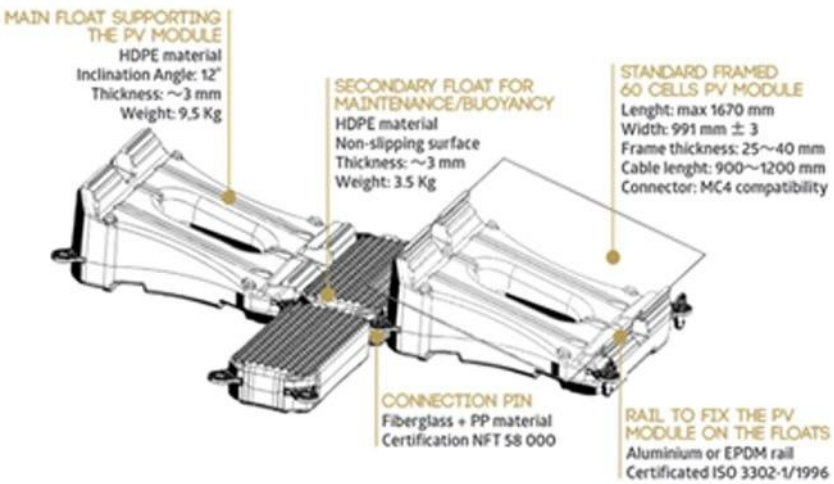

Figure 4.20: Class 2: floater design from Ciel&Terre [22].

Each floater includes a main float and a secondary float, both entirely constructed from HDPE. A mounting rail system made of Aluminium 5005 is used to secure the PV modules. According to Ghigo et al. [9], the aluminium requirement is estimated at 2 kg per module. The material usage and associated costs per floater are summarized in Table 4.8:

Each floater includes a main float and a secondary float, both entirely constructed from HDPE. A mounting rail system made of Aluminium 5005 is used to secure the PV modules. According to Ghigo et al. [9], the aluminium requirement is estimated at 2 kg per

module. The material usage and associated costs per floater are summarized in Table 4.8:

Table 4.8: Cost breakdown of Class 2 materials, including unit price, weight, and total cost

Material	Mass (kg)	Cost (€/kg)	Total Cost (€)
Aliminium 5005	2	2.43	4.86
HDPE	13	4.86	63.86

Given the more intricate geometry of the Hydrelio system and the modular assembly required, an additional 40% manufacturing and assembly overhead is applied. Table 4.9 summarizes the cost breakdown for the Class 2 platform, including material costs and the estimated manufacturing and assembly expenses.

Table 4.9: Total cost summary for Class 2 platform, considering materials and increased manufacturing complexity.

Material/Service	Cost	Unit of Measure
Aliminium 5005	4.86	€
HDPE	63.86	€
Manufacturing work/assemmbly	27.5	€
Total	96.2	€

For Class 2, multiple floats are considered to be connected through pins to form a single platform measuring 10x10, consisting of 100 floats and 100 modules. As such, the total cost of one Class 2 platform is 9,620 €.

4.4.3 Class 3

For the Class 3 system, the platform concept developed by SolarDuck [51], a Dutch company specializing in offshore floating solar technology, is considered. Their full scale pilot features four interconnected triangular platform units, each supported by floating pillars. The structure is entirely made of aluminium, elevating the solar panels and electrical components over three meters above the water surface, providing protection from waves. According to Norsk Hydro [52]—the supplier of the aluminium profiles used in the pilot—each triangular side measures approximately 16 meters, forming a stable and modular offshore solar island. Each paltfrom can host 80 modules.

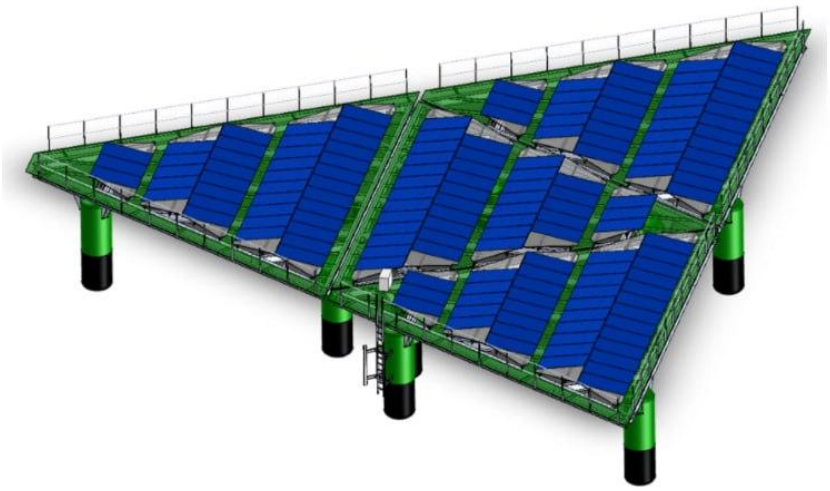

Figure 4.21: Class 3: floater design from SolarDuck [51].

The estimated material usage and associated costs for the Class 3 SolarDuck plat form are summarized in Table 4.10. The structure primarily consists of aluminium, supported by HDPE and stainless steel components.

Table 4.10: Cost breakdown of Class 3 materials, including unit price, weight, and total cost.

Material	Mass (kg)	Cost (€/kg)	Total Cost (€)
Aliminium 5005	3,500	2.43	8,505
HDPE	1,500	1.22	1,830
Steel AISI 205	500	3	1,500

Due to the more complex structure and larger scale of the Class 3 platform, manufacturing and assembly processes are significantly more demanding. As a result, an additional 40% overhead is assumed to account for the increased difficulty in fabrication and transport. Table 6.6 presents the cost breakdown for the Class 3 platform, including individual material costs and the estimated expenses for manufacturing and assembly:

Table 4.11: Total cost summary for Class 3 platform, considering materials and increased manufacturing complexity due to the modular Hydrelio design

Material/Service	Cost	Unit of Measure
Aliminium 5005	8,505	€
HDPE	1,830	€
Stainless Steel	1,500	
Manufacturing work/assemmbly	4,668	€
Total	16,503	€

4.4.4 Mooring and anchoring system

The FPV platforms will use a catenary mooring system, anchored securely to the seabed with drag-embedded anchors. This system design provides the necessary lexibility to withstand varying sea conditions, which is essential for offshore floating PV installations. The mooring chain length lchain is determined by the sea depth Hd, with the total length required being 1.4 times the sea depth. This length is longer than the sea depth by 40% to ensure that the chain is not taut, this slack is necessary to allow free movement of the platform, by doing so the mechanical stresses on the mooring system is reduced [9]. So the chain length can be calculated as follows:

$$l_{chain} = 1.4 \times H_d \quad (4.8)$$

The main properties of the mooring chain summarised in Table refmaterial-chain.

Table 4.12: Summary of the main characteristics of the mooring chain.

Characteristics	Value	Unit of Measure
Diameter	0.03	m
Unit Weight	18.2	kg/m
Cost Steel	2.75	€/kg

Using the available data, the cost of the mooring chain per line is calculated as:

$$C_{chain} = l_{chain} \times 18.2 \times 2.75 \quad (4.9)$$

Where 18.2 is the chain mass per meter [kg/m], and 2.75 is the cost per kilogram [€/kg]. For the drag-embedded anchors, the cost depends on the Minimum Breaking Load (MBL) required by the mooring system. In this study, the MBL is estimated to be 736 kN for all platforms, based on structural constraints and safety considerations [9]. The anchor cost is calculated using the following formula:

$$C_{drag} = 736{,}000 \times \frac{0.052}{9.81} \quad (4.10)$$

Resulting in:

$$C_{drag} = 736{,}000 \times \frac{0.052}{9.81} \approx 3{,}901.32\ € \quad (4.11)$$

Therefore, the total cost of a single mooring line is given by:

$$C_{mooring} = C_{chain} + C_{drag} \quad (4.12)$$

This method offers a robust and detailed approach for estimating the mooring system costs of a generic floating PV platform, accounting for structural flexibility and hydrodynamic motion requirements. Assuming a fixed distance from shore dcoast of 1,000 m and a water depth of 40 m, the chain length per mooring line is set to 56m. The number of mooring lines required varies by platform class:
• Class 1: 1 mooring line per platform
• Class 2: 1 mooring line per aggregated float structure
• Class 3: 2 mooring lines per platform (due to increased structural loads and complexity)
Substituting the values, the mooring cost per line becomes:

$$C_{mooring} = 56 \times 18.2 \times 2.75 + 3{,}901 = 5{,}802\ €/line \quad (4.13)$$

4.4.5 Electrical components

As mentioned in Section above, there are two main layout options for electrical design. First place all the necessary electrical components—such as inverters and transformers—on the floating platforms. In this case, the electricity is converted to AC offshore, and an underwater AC cable is used to transmit it to shore [9].
The alternative approach is to transmit the electricity as DC via a submarine cable and carry out the voltage and frequency conversion at an onshore substation [18].
This study adopts the second option. The costs of the key electrical components are summarized in the Table refcost-eletrical:

Table 4.13: Estimated costs for electrical infrastructure components.

Component	Cost	Unit of Measure
Submarine DC cable	2.18	k€/(MW·km)
On-shore substation	157.36	k€/MW

For a given P_n and $d_{coast,}$ it's possible to determine the total cost of the substation $C_{substation}$ and of the submarine cable C_{cables}:

$$C_{substation} = 157{,}360 \times P_n \quad (4.14)$$

$$C_{cables} = 2.18 \times P_n \times d_{coast} \quad (4.15)$$

For the photovoltaic panel, the SunPower Maxeon 3 model is considered, which has a nominal power of 400W and a cost of 300 € per unit [9]. So, the total cost of the PV modules is evaluated starting from the P_n:

$$C_{PV} = \frac{P_n}{P_{panel}} \times C_{panel} \quad (4.16)$$

Table 4.14: Cost breakdown of Class 2 materials, including unit price, weight and total cost.

Material	Mass (kg)	Cost (€/kg)	Total Cost (€)
Aliminium 5005	2	2.43	4.86
HDPE	13	4.86	63.86

4.5 Energy, Environmental, and Economic Assessment

The economic viability of the project is assessed through the estimation of the Net. Present Value NPV, considering various configurations with different numbers of modules to identify the most profitable option. The NPV is an economic indicator used to evaluate the profitability of a cash flow resulting from a specific investment [53]. It is calculated by summing the discounted net cash flows Bt over the plant's lifetime and subtracting the initial investment cost i , using a nominal discount rate i provided by the investor, since the technology is new, it means it has a high level of risk, an i of 6.4% is chosen [9]:

$$NPV = -I + \sum_{t=1}^{n} \frac{B_t - MC_t}{(1+i)^t} \qquad (4.17)$$

The i corresponds to the capital expenditures CapEx, which are composed of several components:

$$I = CapEx = C_{con} + C_{el} + C_{platform} + C_{mooring} + C_{PV} + C_{installation} \qquad (4.18)$$

Where $C_{platform}$ and $C_{mooring}$ are evaluated through the bottom-up approach. For the project to be economically sustainable, a positive NPV must be achieved.
This indicator is useful for comparing different investment options and quantifying the actual monetary return. The term MC_t accounts for the maintenance cost during each period, which represents the operational expenditures OpEx, and is defined as:

$$MC_t = OpEx = 0.025 \times CapEx \qquad (4.19)$$

In this analysis, the B_t is derived from the avoided cost of electricity that would otherwise be supplied through a combination of grid and diesel generation sources, as shown in eq. 7.4

$$B_t = Energy_t \times C_{kwh} \qquad (4.20)$$

Since the two selected locations (Pantelleria and North Sea) are either island-based or exposed marine zones with potential infrastructure constraints, the cost of electricity C_{kWh} is evaluated under a hybrid supply assumption. Specifically, we assume that

80% of the electricity demand is met by the national grid, while the remaining 20% is produced using diesel generators for backup or peak demand.

According to literature (Casillas et al. [54]), the specific fuel consumption of typical diesel generators (55–110 kW range) falls between 0.41 and 0.52 L/kWh, with an average of 0.465 L/kWh used in this study. The diesel generation cost $C_{\text{diesel-kWh}}$ is calculated using local diesel prices for each site and this conversion factor.

The cost per kilowatt-hour of electricity generated by diesel generator $C_{\text{diesel-kWh}}$ is estimated using the following equation.

$$C_{\text{diesel-kWh}} = C_{\text{diesel}} \times \eta_{diesel} \quad (4.21)$$

Where the average fuel consumption η_{diesel} used for this calculation is:

$$\eta_{\text{diesel}} = \frac{0.41 + 0.52}{2} = 0.465\ L/kWh$$

The final CkWh used in the analysis is calculated as a weighted average, where 80% of the electricity is assumed to come from the grid and 20% from diesel generators:

$$C_{\text{diesel-kWh}} = 0.2\ \times C_{\text{diesel-kWh}} + 0.8 \times C_{grid} \quad (4.22)$$

In this analysis, parameters such as unit selling price, and retail value are assumed to remain constant throughout the system's lifetime. The NPV does not account for uncertainties related to these variables. Based on these assumptions, it is possible to compute the NPV over time and determine the point at which the investment breaks even. This corresponds to the Payback Time tPBT, which is defined as the period required to recover the initial investment through accumulated savings or revenues [53]. The tPBT is determined by the condition:

$$PBT = t_{PBT} \ \rightarrow \ NPV(t_{PBT}) = 0$$

The Levelized Cost of Energy (LCOE) is another critical economic metric used to assess the cost-effectiveness of energy generation. It represents the per-unit cost of energy produced by the system, considering both CapEx and OpEx over the project's lifetime [7]

$$LCOE = \frac{I + \sum_{t=1}^{n} \frac{MC_t}{(1+i)^t}}{\sum_{t=1}^{n} \frac{E_t}{(1+i)^t}} \quad (4.23)$$

4.5.1 Installation Cost

Estimating the installation cost of the floating structure and its mooring system presents a challenge due to the emerging nature of the technology and the limited availability of real-world cost data. To address this, the methodology adopted in [18] is applied. This approach is adapted from offshore wind industry practices and accounts for variables such as vessel chartering, installation time, and travel distance from shore. The installation cost is expressed as:

$$C_{install\ _FPV}(x,y) = n_{FPV}\left[T_{install} + \frac{2d(x,y)}{v_{boat}}\right] \times \frac{C_{boat}+C_{divers}+C_{workers}}{n_{FPV}{}_{petrip}}, \quad (4.24)$$

where:

1. $n_{FPV:}$ total number of floating units to be installed in the project
2. $n_{FPV\_petrip:}$ number of floating units that can be transported and deployed per trip by the installation vessel.
3. $T_{install:}$ time required to install a single FPV unit once on site.
4. d(x,y): distance from the installation site to shore, expressed as a function of its spatial coordinates.
5. V_{boat}: speed of the jack-up vessel used during the transport and installation phases.
6. C_{boat}: daily or hourly charter cost associated with the use of the jack-up vessel.
7. C_{divers}: cost of divers (per unit of time).
8. $C_{workers}$: cost of workers (per unit of time).

The input parameters used in the equation are summarized in Table 4.15:

Table 4.15: Input parameters used for the installation cost estimation.

Symbol	Value	Unit of Measure	Source
η_{FPV}	Depends on system size	-	Assumed
$\eta_{FPV\_pertrip}$	Depends on class type	units/trips	-
$T_{install}$	0.5	hours/unit	-
d(x,y)	-	km	-
v_{boat}	2000	m/h	[18]
C_{boat}	120	€	[58]
C_{divers}	50	€	[58]
$C_{workers}$	90	€	[58]

The $T_{install}$ of each platform and $nF_{PV\_pertrip}$ are assumed by considering the values of deployment of similar off-shore technologies. In the case of Class1 and Class2 we consider 5 units transported per trip, while for class3 we consider 2 platforms per trip. This model enables a more structured and location-sensitive estimation of installation costs for FPV systems, particularly in the absence of historical installation cost data.

4.5.2 Comparative plots

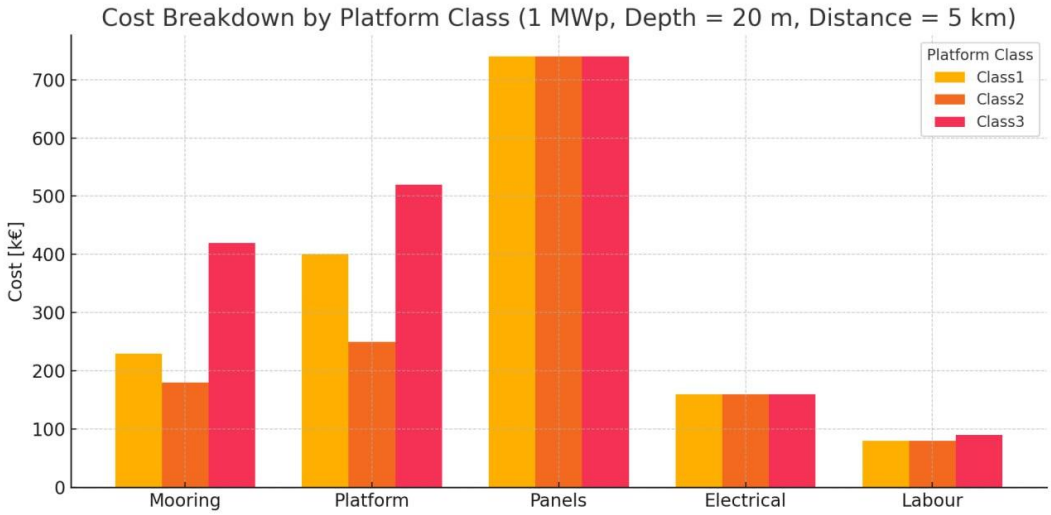

Figure 4.22 Cost Breakdown by Platform Class

Figure 4.21Here is the cost breakdown chart for your three platform classes using fixed parameters from your code (1 MWp system, 20 m depth, 5 km distance). The costs are separated into components—

Mooring, Platform, Panels, Electrical, and Labor—and displayed in thousands of euros (€k).

Figure 4.21 illustrates the absolute cost breakdown (in thousands of euros) of Floating Photovoltaic (FPV) systems across three structural classes—Class 1, Class 2, and Class 3—for a 1 MWp system, assuming fixed environmental conditions (water depth of 20 m and distance to shore of 5 km). The cost components are divided into mooring, platform, panels, electrical infrastructure, and labor.

Despite constant panel and electrical costs across all classes (since these components are independent of structural classification), the figure highlights significant cost variations in mooring and platform structures. Class 3, which includes a composite triangle design with higher structural robustness, incurs the highest mooring and platform costs, followed by Class 1. Class 2, based on simpler pontoons, demonstrates the lowest structural cost contributions, but at the expense of operational resilience. This visualization is crucial in emphasizing the trade-offs between cost and platform durability in varying marine conditions.

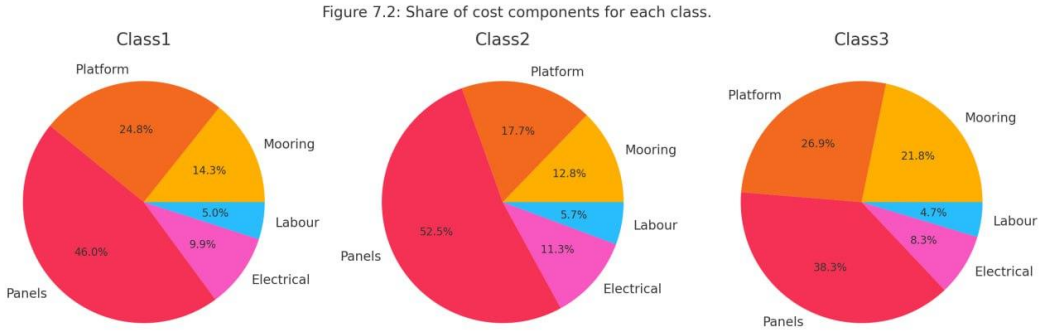

Figure 4.23: Share of cost components for each class.

Figure 4.22 presents the relative share (%) of each cost component within the total system cost for each FPV class. The pie charts normalize the data from Figure 4.21, providing insight into the internal cost structure of each platform configuration.

For Class 1, platform costs dominate (≈25%), while panels contribute nearly half of the total cost. Class 2 shows an even stronger dependence on panel costs (≈56%), making it the most panel-dominated configuration due to reduced structural expenditures. In contrast, Class 3 exhibits a more balanced cost distribution, with mooring (≈18%) and platform (≈27%) taking a more substantial share, reflecting its robustness for harsher sea conditions.

These visualizations support a comparative techno-economic assessment, revealing how class selection affects not only total capital expenditure but also the allocation of investment across different subsystems.

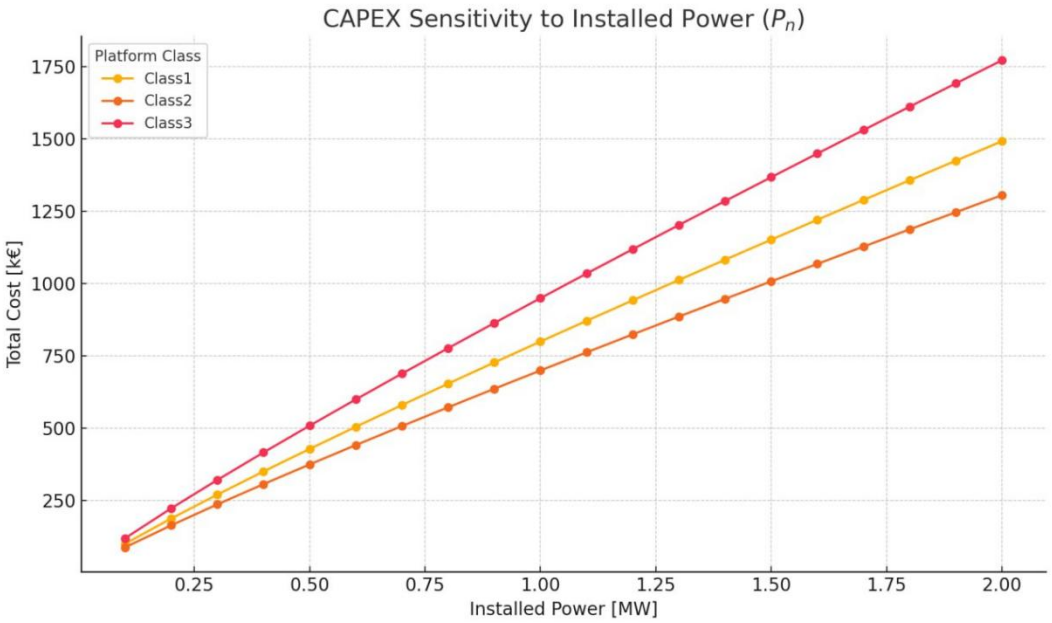

Figure 4.24: CapEx sensitivity to Pn.

The graph shows the capital cost trajectory for each platform class (Class 1, 2, and 3) as the installed power increases from 0.1 MW to 2.0 MW. The cost trend follows a sub-linear scaling governed by the exponent $P^{0.9}$, as implemented in your code.

Class 3 consistently exhibits the highest CAPEX due to more complex structures and higher platform and mooring costs.

Class 2, optimized for cost efficiency, remains the most economical configuration.
The divergence in cost curves widens with increasing system size, reinforcing that scaling up amplifies the economic impact of platform choice.

4.5.3 Economies of Scale in CapEx and OpEx Estimation

To more accurately reflect the behavior of large-scale FPV systems, the cost model integrates the effect of economies of scale. In real-world deployments, unit costs generally decrease as system capacity increases due to improved purchasing power, shared infrastructure, and operational efficiencies.

In this thesis, both capital expenditures (CapEx) and operational expenditures (OpEx) are adjusted using scaling exponents derived from relevant literature on floating solar system design and cost modeling.[61]

The scaled CapEx is given by:

$$CapEx_{total} = CapEx_{unit} \times P_n^{0.9} \qquad (4.25)$$

Similarly, OpEx is scaled by:

$$OpEx_{total} = OpEx_{unit} \times P_n^{0.9} \qquad (4.26)$$

Where P_n is the installed capacity in MW. The exponent value of 0.9 reflects a mild sub-linear relationship (i.e., the cost increases less than proportionally with power capacity). This approach is consistent with commonly adopted methods in the techno-economic evaluation of solar energy systems, particularly in floating and offshore applications.

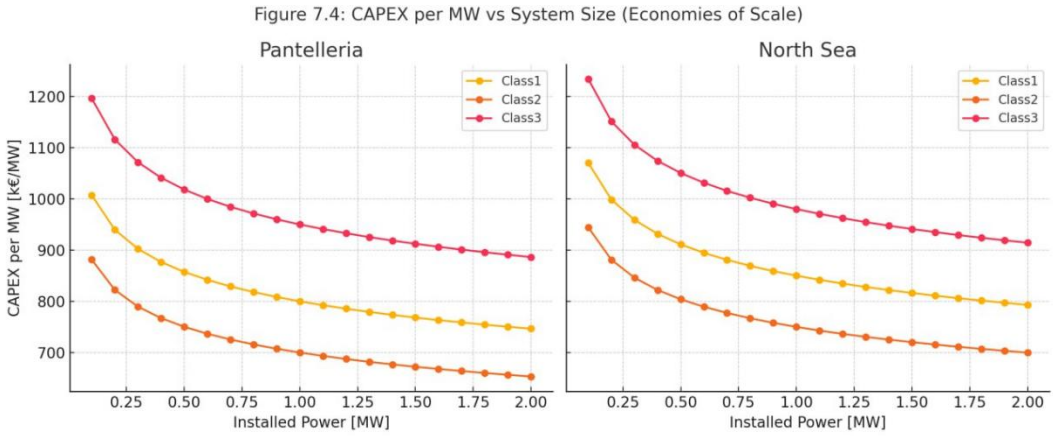

Figure 4.25: CapEx per MW vs. System Size for both Pantelleria and the North Sea.

This figure illustrates the impact of economies of scale on the capital cost per unit of installed capacity for all three FPV platform classes across two locations: Pantelleria (Site A) and the North Sea (Site B). The curves show how CapEx per megawatt (€/MW) decreases with

increasing system size, following a sub-linear scaling law defined by a power exponent of 0.9.

The effect is especially pronounced in the lower capacity range (0.1–1.0 MW), where marginal gains from scaling are strongest. As capacity increases, the CapEx per MW for each class asymptotically approaches a lower bound, demonstrating diminishing returns but still indicating cost advantage at scale.

Pantelleria consistently shows slightly lower unit costs across all classes, mainly due to reduced mooring complexity and labor assumptions. Class 3, being structurally more complex, maintains a higher CapEx baseline, though it too benefits from scale. This figure confirms that system sizing plays a key role in project viability and cost efficiency, particularly for offshore and nearshore applications where fixed overheads and anchoring dominate total expenditure.

4.6 CO2 Emissions Avoided

One of the primary environmental benefits of deploying FPV systems is the reduction in carbon dioxide (tCO2) emissions through the displacement of fossil fuel-based electricity generation. This section quantifies the total tCO2 emissions avoided at each selected location by substituting a portion of the local energy demand with electricity produced by the FPV systems. To estimate the emissions avoided, the analysis assumes that the electricity generated by the FPV system offsets the average local electricity mix, which, in many semi-isolated or island regions, includes a significant share of diesel-based generation. The emissions avoided are calculated using the following expression.

$$CO_{2,avoided} = E_y \times EF_{avg} \quad (4.27)$$

Where EFavg is the average emission factor of the displaced electricity source, expressed in tons of CO2 per megawatt-hour (kgCO2/MWh)

The EFavg used in this analysis are based on a combination of data sources: for electricity from the national grid were retrieved from the public dataset provided by Our World in Data [59], which reports the carbon intensity of electricity generation across countries. For

diesel-based generation, the average emission factor was taken from the study by Jakhrani et al. [60], which assessed the carbon footprint of various diesel generators with different rated powers.

According to their findings, the average EFavg from diesel-based electricity production is estimated at 1.585 kgCO2/kWh. A weighted average EFavg for each location is then calculated based on the assumed energy mix—20% from diesel and 80% from grid electricity—to reflect the hybrid nature of power supply in semi-isolated regions, as done for the energy price in the 7.1.2

$$EF_{avg} = 0.2 \times EF_{diesel} + 0.8 \times EF_{grid} \quad (4.28)$$

In Table 4.16 the results relating to the average emission factor for each location, EFavg, are summarized, where in Et the first year is considered.

Table 4.16: Estimated annual tCO2 emissions avoided by FPV deployment at each location.

Site	E_y (MWh/yr)	EF_{avg} (tCO2/MWh)	tCO2/year avoided
Pantelleria	1462.73	0.547	800.59
North Sea	928.04	0.357	331.32

The analysis shows that the FPV system deployed in Pantelleria has a significantly higher CO_2 offset compared to the same system in the North Sea. This is primarily due to:

A higher solar yield (leading to more energy production),

And a dirtier grid mix in southern Italy versus offshore Dutch power, which is already heavily decarbonized.

These findings underline the dual environmental and economic benefits of deploying FPV in semi-isolated, diesel-dependent regions. They also reinforce the policy case for prioritizing renewable investments in areas with higher marginal carbon intensity.

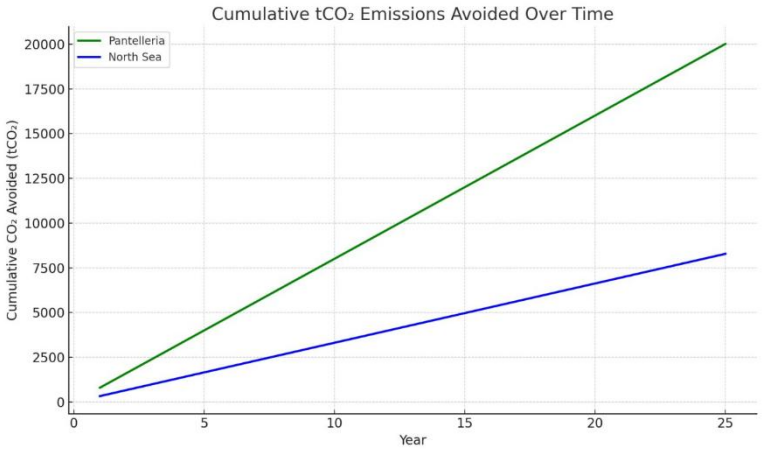

Figure 4.26 Cumulative tCo2 emissions avoided overtime

Here's the plot illustrating the cumulative tons of CO_2 emissions avoided over a 25-year period for the two selected locations—Pantelleria and the North Sea site:

Figure: Cumulative tCO_2 Emissions Avoided Over Time
Pantelleria starts with a higher annual CO_2 displacement (800.59 tCO_2/year), which results in significantly greater cumulative avoided emissions.

North Sea exhibits a more modest CO_2 displacement rate (331.32 tCO_2/year), reflecting its cleaner baseline energy mix and lower solar yield.

Summary

This chapter synthesizes the analytical results and visualization outputs from the preceding technical and economic modeling. While Chapters 5 through 7 focused on energy estimation, cost structure, and financial indicators, here we consolidate those findings and provide additional interpretations to highlight comparative strengths and weaknesses of the two locations (Pantelleria and North Sea) and three platform classes.

Table 5.1 summarizes the energy and economic results for both Pantelleria (Site A) and North Sea (Site B)—at three system sizes: 1 MW, 10 MW, and 100 MW. Values are derived from the techno-economic model using fixed assumptions: 20 m bathymetry depth, 5 km distance to shore, and site-specific irradiance and environmental metrics.

Table 5.1 Key metrics for 1Mwh

Site	Class	Energy (MWh/yr)	CapEx (€M)	NPV (€M)	LCOE (€/MWh)	Payback (yr)
Pantelleria	Class 1	1462.73	1.093	0.686	65.84	10
Pantelleria	Class 2	1316.46	1.189	0.412	77.57	14
Pantelleria	Class 3	1609.00	1.530	0.406	82.04	15
North Sea	Class 1	928.04	1.093	-0.039	103.78	None
North Sea	Class 2	835.24	1.189	-0.240	122.27	None
North Sea	Class 3	1020.85	1.530	-0.391	129.31	None

At 1 MW scale, the results highlight substantial differences between the two sites. Pantelleria significantly outperforms the North Sea across all platform classes in terms of net present value (NPV), levelized cost of energy (LCOE), and payback period. For instance, Class 1 in Pantelleria achieves an LCOE of €65.84/MWh and a

payback of 10 years, while the same class in the North Sea results in a much higher LCOE of €103.78/MWh with no payback within the project lifetime.

These discrepancies are largely driven by environmental differences—Pantelleria benefits from higher solar irradiance and calmer sea conditions, leading to greater energy production and lower capital risks. In contrast, the North Sea's harsher wave regime and lower solar yield reduce both technical and financial performance at small scale.

Table 5.2 Key metrics for 10Mwh

Site	Class	Energy (MWh/yr)	CapEx (€M)	NPV (€M)	LCOE (€/MWh)	Payback (yr)
Pantelleria	Class 1	14627.32	8.711	9.495	52.45	7
Pantelleria	Class 2	13164.58	9.475	6.910	61.79	10
Pantelleria	Class 3	16090.05	12.196	7.669	65.36	10
North Sea	Class 1	9280.45	8.711	2.250	82.67	16
North Sea	Class 2	8352.40	9.475	0.389	97.39	22
North Sea	Class 3	10208.49	12.196	-0.300	103.01	None

As capacity increases to 10 MW, economies of scale begin to take effect. Both sites show improved financial viability, although Pantelleria still leads in all classes. Class 1 sees its LCOE drop to €52.45/MWh in Pantelleria and €82.67/MWh in the North Sea. Payback periods also shorten, most notably for Class 1 in Pantelleria (7 years), reinforcing its suitability for cost-effective deployment.

Interestingly, Class 3 in the North Sea remains financially infeasible at this scale (NPV still negative), suggesting that more structurally robust platforms require either higher capacity or more favorable conditions to break even.

Table 5.3 Key metrics for 100Mwh

Site	Class	Energy (MWh/yr)	CapEx (€M)	NPV (€M)	LCOE (€/MWh)	Payback (yr)
Pantelleria	Class 1	146273.17	69.199	116.182	41.67	5
Pantelleria	Class 2	131645.85	75.269	91.574	49.08	7
Pantelleria	Class 3	160900.48	96.879	105.758	51.92	7

North Sea	Class 1	92804.47	69.199	43.730	65.67	10
North Sea	Class 2	83524.02	75.269	26.367	77.36	14
North Sea	Class 3	102084.92	96.879	26.061	81.83	15

At 100 MW, the impact of scaling becomes fully apparent. Every configuration, including those previously unprofitable, becomes viable. For example, Class 1 in the North Sea, which failed to repay in 25 years at 1 MW, achieves a 10-year payback and an LCOE of €65.67/MWh at 100 MW. Pantelleria achieves peak performance here, with Class 1 delivering an LCOE as low as €41.67/MWh and an NPV exceeding €116 million.

The results confirm that system scale is a decisive factor for project viability, particularly in offshore or harsher environments. While Pantelleria remains superior across all classes and sizes, even the North Sea becomes financially attractive when leveraging large-scale installations and the resulting cost dilution.

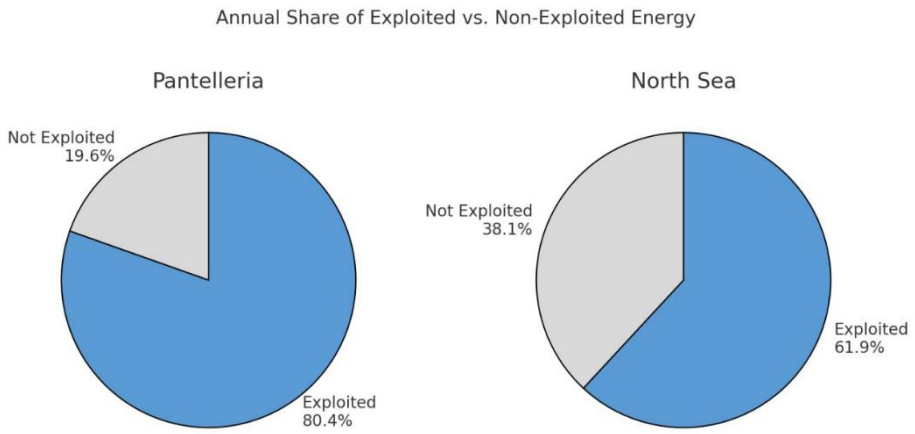

Figure 5.1 Annual share of exploited vs non-exploited Energy

Here is the figure showing the annual share of exploited vs. non-exploited energy due to solar radiation (SR) for both locations:

Pantelleria exhibits high solar utilization, with approximately 80.4% of the potential solar energy being exploited.

North Sea shows a lower utilization rate, with only 61.9% of the potential solar radiation being harnessed, and 38.1% remaining unused due to lower irradiance or inefficiencies.

Interpretation of Class Performance

Class 1 platforms consistently yield the fastest payback and lowest LCOE at both sites, making them attractive for cost-sensitive deployments in moderate wave conditions.
Class 3, while more expensive, delivers higher energy output and long-term revenue potential, particularly in environments where structural resilience is critical.

Pantelleria's higher solar resource offsets its higher diesel-grid cost mix, producing more favorable economic metrics overall.

Comparison and Deployment Recommendations

Pantelleria outperforms the North Sea across all financial metrics, mainly due to stronger irradiance and calmer sea conditions.
The North Sea, while more structurally demanding, can justify higher-class investments if subsidy frameworks or hybrid configurations are available.
For scalability beyond 1 MW, both locations benefit from significant cost reductions per MW, as confirmed in the CAPEX scaling plots.

The comparative techno-economic analysis performed in this thesis demonstrates the compelling case for floating photovoltaic (FPV) systems in both moderate and challenging marine environments. Through the integration of detailed environmental datasets, bottom-up cost modeling, and scalable performance metrics, we assessed three distinct platform classes across two geographically and climatically different locations: Pantelleria in the Mediterranean Sea and the North Sea above the West Frisian Islands.

At lower capacities (1 MW), only favorable irradiance and calm sea conditions (as found in Pantelleria) yielded economically viable configurations. However, as installed capacity scaled to 10 MW and 100 MW, even harsher environments (e.g., the North Sea) became financially attractive, driven by economies of scale and class-specific performance gains.

From a technology perspective, Class 1 platforms (modular floats) consistently performed best in terms of payback and LCOE, while Class 3 systems (triangular pontoons) excelled in yield but required higher upfront investment. Class 2 served as a balanced intermediary. Environmental conditions—particularly irradiance,

wave period, and water depth—strongly influenced performance-class matching.

The model's flexibility allows for site-specific evaluation of structural costs, energy production, and financial returns under different assumptions, making it a robust planning tool for developers and policymakers.

Future Outlook

Looking ahead, FPV technology is expected to play a central role in offshore energy strategies due to its:

Minimal land use footprint and land-use conflict

Synergies with hydropower, aquaculture, and coastal protection systems

Potential for high scalability in sheltered seas and nearshore regions

To further develop FPV viability and competitiveness, several avenues are worth pursuing:

Design optimization: Advanced structural modeling and material innovation can reduce platform and mooring costs.

Digital twins: Real-time performance tracking integrated with predictive maintenance can reduce O&M costs.

Hybridization: Coupling FPV with storage or wind systems can mitigate intermittency and improve grid stability.

Policy support: Targeted incentives, streamlined permitting, and integration with blue economy initiatives will accelerate deployment.

With its expanding commercial interest and alignment with global decarbonization goals, offshore FPV represents one of the most promising frontiers in the solar energy landscape. The findings of this thesis not only highlight current technological and economic potential but also pave the way for scalable, resilient, and environmentally sound energy solutions in coastal and offshore zones.

Appendices

Appendix A – FPV Techno-Economic Model: User Manual

1. Overview
This manual describes a Python-based techno-economic model for evaluating floating photovoltaic (FPV) energy systems. It integrates environmental data retrieval, energy yield estimation, and economic analysis to assess the viability of FPV installations at specified marine locations.

2. Script Structure
The script is structured into the following components:
- Main Script: Coordinates user inputs and model execution.
- DynamicFPVCostModel class: Performs all calculations related to cost, energy, and finance.
- Environmental Data Functions: Download and process ERA5 data.
- Helper functions: Load ports, find closest port, etc.

3. Environmental Metrics
Environmental inputs include significant wave height, wave period, wind speed, and bathymetry. These are retrieved using ERA5 datasets and used to classify the site into one of three environmental classes (Class1, Class2, Class3).

4. Energy Production
Energy yield is estimated to be based on surface solar radiation data. The model uses standard efficiency and performance ratio assumptions and adjusts for technology-specific factors.

5. Cost and Financial Analysis
The model calculates:
- CAPEX and OPEX based on component cost breakdowns
- Levelized Cost of Energy (LCOE)
- Net Present Value (NPV)
- Internal Rate of Return (IRR)
- Payback Period

6. Technology Classes
The model supports three environmental technology classes:
- Class1: Baseline
- Class2: Reduced energy and OPEX factor
- Class3: Higher CAPEX and energy factor

7. Required Python Libraries

Ensure the following Python packages are installed:
- cdsapi
- xarray
- numpy
- pandas
- geopy
- shapely
- geopandas

8. Usage Instructions
Run the script in a Python environment. You'll be prompted for inputs:
Latitude, Longitude, Capacity (MW), Box size (deg), Year, and Technology type.

Example:
Latitude: 38.5
Longitude: -9.1
Capacity [MW]: 5
Box size [deg]: 0.1
Year: 2023
Technology: Bifacial PV

Appendix B - Python scripts of the tool

```python
class DynamicFPVCostModel:
    def __init__(
        self, lat, lon, box_size, year, capacity_mw, technology,
        ports_csv=PORTS_CSV_PATH, price_per_mwh=100.0,
        life_time=25, discount_rate=0.06,
        fixed_depth=None, fixed_distance=None,
        capex_exp=0.9, opex_exp=0.9
    ):
        self.lat = lat; self.lon = lon
        half = box_size / 2
        self.bbox = [lat+half, lon-half, lat-half, lon+half]
        self.year = year
        self.capacity_mw = capacity_mw
        self.tech = technology
        self.price_per_mwh = price_per_mwh
        self.life_time = life_time
        self.r = discount_rate
        self.fixed_depth = fixed_depth
        self.fixed_distance = fixed_distance
        self.capex_exp = capex_exp
        self.opex_exp  = opex_exp
        self.cds = cdsapi.Client()
        df = pd.read_csv(ports_csv)
        df['geometry'] = df.apply(lambda r: Point(r.Longitude, r.Latitude), axis=1)
        self.ports_gdf = gpd.GeoDataFrame(df, geometry='geometry')
```

```python
def _fetch_mean(self, variable, varname=None, annual_sum=False):
    with tempfile.NamedTemporaryFile(suffix='.nc', delete=False) as tf:
        fn = tf.name
    if variable == 'surface_solar_radiation_downwards':
        self.cds.retrieve(
            'reanalysis-era5-single-levels-monthly-means',
            { 'product_type':'monthly_averaged_reanalysis', 'format':'netcdf',
              'variable':[variable], 'year':self.year,
              'month':[f"{m:02d}" for m in range(1,13)], 'time':'00:00',
              'area':self.bbox },
            fn
        )
        ds = xr.open_dataset(fn, decode_times=True)
        arr = ds[varname] if varname else ds[list(ds.data_vars)[0]]
        td = next((d for d in arr.dims if np.issubdtype(ds[d].dtype, np.datetime64)), None)
        days = xr.DataArray(ds[td].dt.daysinmonth, coords={td: ds[td]}, dims=[td])
        val = float((arr * days).sum(dim=td).item())
        ds.close(); os.remove(fn)
        return val
```

```
    else:
        self.cds.retrieve(
            'reanalysis-era5-single-levels',
            { 'product_type':'reanalysis', 'format':'netcdf',
              'variable':[variable], 'year':self.year,
              'month':[f"{m:02d}" for m in range(1,13)],
              'day':[f"{d:02d}" for d in range(1,32)],
              'time':['12:00'], 'area':self.bbox },
            fn
        )
        ds = xr.open_dataset(fn, decode_times=True)
        arr = ds[varname] if varname else ds[list(ds.data_vars)[0]]
        td = next((d for d in arr.dims if 'time' in d.lower()), None)
        if td:
            val = float(arr.resample({td:'1Y'}).sum().item()) if annual_sum else float(arr.resample({td:'1Y'}).me
        else:
            val = float(arr.sum().item()) if annual_sum else float(arr.mean().item())
        ds.close(); os.remove(fn)
        return val
```

```
def mean_ssrd_J(self):
    return self._fetch_mean('surface_solar_radiation_downwards', 'ssrd', annual_sum=True)

def mean_depth(self):
    return self.fixed_depth if self.fixed_depth is not None else self._fetch_mean('model_bathymetry', 'wmb')

def distance_to_shore(self):
    if self.fixed_distance is not None:
        return self.fixed_distance
    return float(self.ports_gdf.geometry.apply(lambda pt: geodesic((self.lat, self.lon), (pt.y, pt.x)).km).min())

def compute_energy_production(self, eta_stc=0.20, perf_ratio=0.80):
    ssrd = self.mean_ssrd_J() / 3.6e6
    area = self.capacity_mw * 1e6 / (1000 * eta_stc)
    base = ssrd * eta_stc * perf_ratio * area
    return base * energy_factor.get(self.tech, 1.0) / 1e3  # MWh/yr

def design(self, depth):
    Nmod = self.capacity_mw * 1e3 / 0.4
    Nplt = int(Nmod / 70)
    chain = depth * 1.4
    return Nmod, Nplt, chain
```

```
def mooring_cost(self, Nplt, chain):
    fac = { 'Fixed':1, 'Dual-Axis Tracking System':2.15, 'Bifacial PV':1.15, 'Active Cooling':1.2 }
    return (chain * 18.2 * 2.75 * Nplt + 736000 * 0.052 / 9.81 * Nplt) * fac.get(self.tech,1)

def platform_cost(self, cls, Nplt):
    if cls == 'Class2':
        return self.capacity_mw * 1e3 * COST_PER_FLOAT
    if cls == 'Class3':
        return Nplt * COST_PER_TRIANGLE
    return 0

def panel_cost(self, Nmod):
    return Nmod * 300

def electrical_cost(self, dist):
    return 157360 * self.capacity_mw + 2.18 * dist * self.capacity_mw

def opex(self):
    base = self.capacity_mw * 15_000
    # sub-linear or linear OPEX
    return (base * opex_factor.get(self.tech,1.0) ** 1) * (self.capacity_mw ** (self.opex_exp-1)) / 1e3
```

(variable) capacity_mw: Any

```python
def compute_financials(self, production_mwh):
    depth = self.mean_depth()
    Nmod, Nplt, chain = self.design(depth)
    raw_capex = (
        self.mooring_cost(Nplt, chain)
      + self.platform_cost(self.tech, Nplt)
      + self.panel_cost(Nmod)
      + self.electrical_cost(self.distance_to_shore())
    )
    unit_cap = raw_capex / self.capacity_mw
    capex    = unit_cap * (self.capacity_mw ** self.capex_exp)

    years      = np.arange(self.life_time)
    revenue    = [m * self.price_per_mwh for m in production_mwh]
    opx        = [self.opex() * 1000 for _ in years]
    cashflow   = [r - o for r, o in zip(revenue, opx)]
    discounted= [cf / ((1 + self.r) ** yr) for yr, cf in zip(years, cashflow)]
    discounted[0] -= capex
    cumulative= np.cumsum(discounted)
```

```python
        return pd.DataFrame({
            'Year': years,
            'CapEx': [capex] + [0]*(self.life_time-1),
            'Revenue': revenue,
            'OpEx': opx,
            'Cashflow': cashflow,
            'DiscountedCashflow': discounted,
            'CumulativeNPV': cumulative
        })

    def payback_time(self, production_mwh):
        df = self.compute_financials(production_mwh)
        repay = df.loc[df['CumulativeNPV'] >= 0, 'Year']
        return int(repay.iloc[0]) if not repay.empty else None

    def lcoe(self, production_mwh):
        df = self.compute_financials(production_mwh)
        disc_op  = df['OpEx'][1:] / ((1 + self.r) ** df['Year'][1:])
        disc_en  = [m / ((1+self.r)**y) for y,m in zip(df['Year'], production_mwh)]
        cap      = df['CapEx'].iloc[0]
        return (cap + disc_op.sum()) / sum(disc_en[:-1])
```

```python
    def irr(self, production_mwh=None, df=None):
        if df is None:
            if production_mwh is None:
                raise ValueError("Must provide either production_mwh or df.")
        df = self.compute_financials(production_mwh)
        return npf.irr(df['Cashflow'].values)
# ——————————————————————————————————————————————————————————————
```

```python
if Hs < 1.47 or Tp_local < 5.5 or ws < 6.0:
    env_class = 'Class2'
elif 1.47 <= Hs < 2.08 or 5.5 <= Tp_local < 7.0 or 6.0 <= ws < 8.0:
    env_class = 'Class1'
elif 2.08 <= Hs <= 4.03 or Tp_local >= 7.0 or ws >= 8.0:
    env_class = 'Class3'
else:
    env_class = 'Unclassified'
print(f"Assigned Environmental Class: {env_class}")
```

Bibliography

[1] Sanja Filipović, Noam Lior, and Mirjana Radovanović. «The green deal just transition and sustainable development goals Nexus». In: Renewable and Sustainable Energy Reviews 168 (2022), p. 112759. issn: 1364-0321.doi: https://doi.org/10.1016/j.rser.2022.112759. url:https://www.sciencedirect.com/science/article/pii/S1364032122200644X (cit. on p. 1).

[2] Paolo Venturini, Gabriele Guglielmo Gagliardi, Giuliano Agati, Luca Cedola, Michele Vincenzo Migliarese Caputi, and Domenico Borello. «Integration of Floating Photovoltaic Panels with an Italian Hydroelectric Power Plant». In: Energies 17.4 (2024). issn: 1996-1073. url: https://www.mdpi.com/1996 1073/17/4/851 (cit. on pp. 1, 2, 4).

[3] M. López, F. Soto, and Z.A. Hernández. «Assessment of the potential of floating solar photovoltaic panels in bodies of water in mainland Spain».
In: Journal of Cleaner Production 340 (2022), p. 130752. issn: 0959-6526. doi: https://doi.org/10.1016/j.jclepro.2022.130752. url: https://www.sciencedirect.com/science/article/pii/S0959652622003912(cit. on pp. 1, 2).

[4] Alok Sahu, Neha Yadav, and K. Sudhakar. «Floating photovoltaic power plant: A review». In: Renewable and Sustainable Energy Reviews 66 (2016), pp. 815–824. issn: 1364-0321. doi: https://doi.org/10.1016/j.rser. 2016.08.051. url: https://www.sciencedirect.com/science/article pii/S1364032116304841 (cit. on pp. 1, 4).

[5] Adimas Pradityo Sukarso and Kyung Nam Kim. «Cooling Effect on the Floating Solar PV: Performance and Economic Analysis on the Case of West Java Province in Indonesia». In: Energies 13.9 (2020). issn: 1996 1073. doi: 10.3390/en13092126. url: https://www.mdpi.com/1996 1073/13/9/2126 (cit. on pp. 1, 34).

[6] Christopher Small and Robert J. Nicholls. «A Global Analysis of Human Settlement in Coastal Zones». In: Journal of Coastal Research 19.3 (2003), pp. 584–599. issn: 07490208, 15515036. url: http://www.jstor.org/stable/4299200 (visited on 04/23/2025) (cit. on p. 1).

[7] Sara Oliveira-Pinto and Jasper Stokkermans. «Assessment of the potential of different floating solar technologies– Overview and analysis of different case studies». In: Energy Conversion and Management 211 (2020), p. 112747. issn: 0196-8904. doi: https://doi.org/10.1016/j.enconman.2020. 112747. url: https://www.sciencedirect.com/science/article/pii/S0196890420302855 (cit. on pp. 2, 6, 47).

[8] Shiva Gorjian, H. Sharon, Hossein Ebadi, Karunesh Kant, Fausto Bontempo

Scavo, and Giuseppe Marco Tina. «Recent technical advancements, economics and environmental impacts of floating photovoltaic solar energy conversion systems». In: Journal of Cleaner Production 278 (2021), p. 124285. issn: 0959-6526. doi: https://doi.org/10.1016/j.jclepro.2020.124285. url:

https://www.sciencedirect.com/science/article/pii/S095965262034 3304 (cit. on p. 2).
[9] Alberto Ghigo, Emilio Faraggiana, Massimo Sirigu, Giuliana Mattiazzo, and Giovanni Bracco. «Design and Analysis of a Floating Photovoltaic System for Offshore Installation: The Case Study of Lampedusa». In: Energies 15.23 (2022). issn: 1996-1073. doi: 10.3390/en15238804. url: https://www. mdpi.com/1996-1073/15/23/8804 (cit. on pp. 2, 5–7, 37, 40, 42–45).
[10] R. Claus and M. López. «Key issues in the design of floating photovoltaic structures for the marine environment». In: Renewable and Sustainable Energy Reviews 164 (2022), p. 112502. issn: 1364-0321. doi: https://doi.org/
10.1016/j.rser.2022.112502. url: https://www.sciencedirect.com/ science/article/pii/S1364032122004063 (cit. on pp. 4–9, 38).
[11] Paul Rappaport. «The photovoltaic effect and its utilization». In: Solar Energy 3.4 (1959), pp. 8–18. issn: 0038-092X. doi: https://doi.org/10.1016/0038
092X(59)90002-7. url: https://www.sciencedirect.com/science/ article/pii/0038092X59900027 (cit. on p. 5).
[12] Kim Trapani and Dean L. Millar. «The thin film flexible floating PV (T3F-PV) array: The concept and development of the prototype». In: Renewable Energy 71 (2014), pp. 43–50. issn: 0960-1481. doi: https://doi.org/10.1016/j.
renene.2014.05.007. url: https://www.sciencedirect.com/science/ article/pii/S0960148114002584 (cit. on p. 5).
[13] Sara Oliveira-Pinto and Jasper Stokkermans. «Marine floating solar plants: an overview of potential, challenges and feasibility». In: Proceedings of the Institution of Civil Engineers- Maritime Engineering 173.4 (2020), pp. 120 135. issn: 1741-7597. doi: https://doi.org/10.1680/jmaen.2020.10. url:
https://www.sciencedirect.com/science/article/pii/S1741759720 000110 (cit. on p. 5).
[14] Balázs Endrődi, Cintia Alexandra Trapp, István Szén, Imre Bakos, Miklós Lukovics, and Csaba Janáky. «Challenges and Opportunities of the Dynamic Operation of PEM Water Electrolyzers». In: Energies 18.9 (2025). issn: 1996-1073. doi: 10.3390/en18092154. url: https://www.mdpi.com/1996
1073/18/9/2154 (cit. on pp. 5, 7–9, 24).
[15] Hesan Ziar, Bjorn Prudon, Fen-Yu Lin, and Bart Roeffen. «Innovative Floating Bifacial Photovoltaic Solutions for Inland Water Areas». In: Progress in Photovoltaics 29.7 (2020). url: https://www.mdpi.com/1996-1073/18/9/ 2154 (cit. on p. 5).

[16] Swati S Gurfude and P S Kulkarni. «Energy Yield of Tracking Type Floating Solar PV Plant». In: 2019 National Power Electronics Conference (NPEC). 2019, pp. 1–6. doi: 10.1109/NPEC47332.2019.9034846 (cit. on p. 5).
[17] Giuseppe Marco Tina, Fausto Bontempo Scavo, Leonardo Micheli, and Marco Rosa-Clot. «Economic comparison of floating photovoltaic systems with tracking systems and active cooling in a Mediterranean water basin». In: Energy for Sustainable Development 76 (2023), p. 101283. issn: 0973-0826. doi: https://doi.org/10.1016/j.esd.2023.101283. url: https://www.sciencedirect.com/science/article/pii/S0973082623 00140 (cit. on p. 5).
[18] A. Martinez and G. Iglesias. «Mapping of the levelised cost of energy from floating solar PV in coastal waters of the European Atlantic, North Sea and Baltic Sea». In: Solar Energy 279 (2024), p. 112809. issn: 0038-092X. doi: https://doi.org/10.1016/j.solener.2024.112809. url: https: //www.sciencedirect.com/science/article/pii/S0038092X2400504 8 (cit. on pp. 6, 44, 47, 48).
[19] Pietro Elia Campana, Louise Wästhage, Worrada Nookuea, Yuting Tan, and Jinyue Yan. «Optimization and assessment of floating and floating tracking PV systems integrated in on- and off-grid hybrid energy systems.
In: Solar Energy 177 (2019), pp. 782–795. issn: 0038-092X. doi: https://doi.org/10.1016/j.solener.2018.11.045. url: https://www. sciencedirect.com/science/article/pii/S0038092X18311459 (cit. on p. 6).
[20] DNV GLAS. Recommended Practice DNVGL-RP-0584: Design, Development and Operation of Floating Solar Photovoltaic Systems. Technical Report. DNV GL AS, 2021 (cit. on p. 7).

[21] Sun-Hee Kim, Seung-Cheol Baek, Ki-Bong Choi, and Sung-Jin Park. «Design and Installation of 500-kW Floating Photovoltaic Structures Using High Durability Steel». In: Energies 13.19 (2020). issn: 1996-1073. doi: 10.3390/en13194996. url: https://www.mdpi.com/1996-1073/13/19/4996 (cit. on p. 8).
[22] Ciel & Terre. Hydrelio®: the patented floating PV system. https://www.ciel-et-terre.net/hydrelio-floating-solar-technology/hydrelio products/. Accessed: 2025-04-24. 2011 (cit. on pp. 8, 39).
[23] E. Bellini. Floating PV in the Persian Gulf. https://www.pv-magazine.com/2020/02/17/floating-pv-in-the-persian-gulf/. PV Magazine, Accessed: 2025-04-24. 2020 (cit. on p. 8).
[24] J. Scully. Chenya Energy eyes floating PV growth after completing 181MWp offshore project. https://www.pv-tech.org/chenya-energy-eyes-floating-pv-growth-after-completing-181mwp-offshore-project. PV Tech, Accessed: 2025-04-24. 2021 (cit. on p. 8).

[25] Oceans of Energy. North Sea 1 Offshore Solar Project. https://oceansofenergy.blue/north-sea-1-/. Accessed: 2025-04-24. 2025 (cit. on p. 9).
[26] K. N. Sheeba, R. Madhusudhana Rao, and S. Jaisankar and. «A Study on the Underwater Performance of a Solar Photovoltaic Panel». In: Energy Sources, Part A: Recovery, Utilization, and Environmental Effects 37.14 (2015), pp. 1505–1512. doi: 10.1080/15567036.2011.619632. eprint: https: //doi.org/10.1080/15567036.2011.619632. url: https://doi.org/10.1080/15567036.2011.619632 (cit. on p. 9).
[27] Kim Trapani and Dean L. Millar. «The thin film flexible floating PV (T3F-PV) array: The concept and development of the prototype». In: Renewable Energy 71 (2014), pp. 43–50. issn: 0960-1481. doi: https://doi.org/10.1016/j. renene.2014.05.007. url: https://www.sciencedirect.com/science/article/pii/S0960148114 002584 (cit. on p. 9).
[28] Ocean Sun AS. Ocean Sun: Towards a Clean Energy Future. https://oceansun.no/. Accessed: 2025-04-24. 2025 (cit. on p. 9).
[29] P. Sánchez Molina and E. Bellini. CIGS Solar Panels for Offshore PV. https://www.pv-magazine.com/2021/12/01/cigs-solar-panels-for-offshor e-pv/. PV Magazine, Accessed: 2025-04-24. 2021 (cit. on p. 9).
[30] David Firnando Silalahi and Andrew Blakers. «Global Atlas of Marine Floating Solar PV Potential». In: Solar 3.3 (2023), pp. 416–433. issn: 2673 9941. doi: 10.3390/solar3030023. url: https://www.mdpi.com/2673 9941/3/3/23 (cit. on pp. 10, 11).
[31] In:(). url: https://www.ecmwf.int/en/forecasts/dataset/ecmwf reanalysis-v5 (cit. on pp. 10, 23).
[32] Francesco Barbariol, Silvio Davison, Francesco Marcello Falcieri, Rossella Ferretti, Antonio Ricchi, Mauro Sclavo, and Alvise Benetazzo. «Wind Waves in the Mediterranean Sea: An ERA5 Reanalysis Wind-Based Climatology». In: Frontiers in Marine Science Volume 8- 2021 (2021). issn: 2296-7745. doi: 10.3389/fmars.2021.760614. url: https://www.frontiersin.org/ journals/marine-science/articles/10.3389/fmars.2021.760614 (cit. on pp. 10–12).
[33] EMODnet. EMODnet Bathymetry Viewer. Accessed: 2025-04-24. 2025. url: https://emodnet.ec.europa.eu/geoviewer/ (cit. on pp. 13, 16).
[34] C Montero. «Solutions for electricity provision in the off-grid autonomous city of Ceuta (Spain)». In: Master. university of Strathclyde (2018) (cit. on p. 14).
[35]OpenStreetMap contributors. OpenStreetMap. https://www.openstreetmap.org. Accessed: 2025-06-29. 2025 (cit. on pp. 14, 15, 17–19).
[36] Miquel Àngel Martínez-Medina, Miguel Ángel Pérez-Martín, and Teodoro Estrela. «Desalination in Spain and the Role of Solar Photovoltaic Energy». In: Journal of Marine Science and Engineering

12.6 (2024). issn: 2077-1312. url: https://www.mdpi.com/2077-1312/12/6/859 (cit. on p. 15).
[37] Daniele Mosso, Luca Rajteri, and Laura Savoldi. «Integration of Land Use Potential in Energy System Optimization Models at Regional Scale: The Pantelleria Island Case Study». In: Sustainability 16.4 (2024), p. 1644 (cit. on p. 15).
[38] Riccardo Novo, Francesco Demetrio Minuto, Giovanni Bracco, Giuliana Mattiazzo, Romano Borchiellini, and Andrea Lanzini. «Supporting decarbonization strategies of local energy systems by de-risking investments in renewables: a case study on pantelleria island». In: Energies 15.3 (2022), p. 1103 (cit. on pp. 15, 16).
[39] Regione Siciliana- Dipartimento dell'Acqua e dei Rifiuti. Relazione Tecnica:
Impianto di Dissalazione a Pantelleria. Accessed: 2025-07-01. 2013.
url:https://pti.regione.sicilia.it/portal/page/portal/PIR_PORTALE/PIR_LaStrutturaRegionale/PIR_AssEnergia/PIR_Dipartimentodellacquaedeirifiuti/PIR_Bandi/PIR_20131118IMPIANTODISSALAZIONEPANTELLERIA/Relazione%20Dissalatore%20Pantelleria.pdf (cit. on p. 16).
[40] Paola Badurina, Marijan Cukrov, and Čedomir Dundović. «Contribution to the implementation of "Green Port" concept in Croatian seaports». In: Pomorstvo 31.1 (2017), pp. 10–17 (cit. on pp. 16, 17).
[41] Faten Attig-Bahar, Uwe Ritschel, Peter Akari, Ibrahim Abdeljelil, and Mahbouba Amairi. «Wind energy deployment in Tunisia: Status, Drivers, Barriers and Research gaps—A Comprehensive review». In: Energy Reports 7 (2021), pp. 7374–7389. issn: 2352-4847. doi: https://doi.org/10.1016/j.egyr.2021.10.087. url:https://www.sciencedirect.com/science/article/pii/S2352484721011057 (cit. on p. 18).
[42] Roukaya Issaoui, Christine Rösch, Jörg Woidasky, Mario Schmidt, and Tobias Viere. «Cradle-to-gate life cycle assessment of beneficiated phosphate rock production in Tunisia [Ökobilanz der Produktion von aufbereitetem Phosphat gestein in Tunesien (von der Wiege bis zu Bahre)]». In: Sustainability Nexus Forum 29.2 (June 2021), pp. 107–118. doi: 10.1007/s00550-021-00522-8. url: https://ideas.repec.org/a/spr/sumafo/v29y2021i2d10.1007_s00550-021-00522-8.html (cit. on p. 18).
[43] Khaoula Daghsen, Dorra Lounissi, and Nahla Bouaziz. «A universal model for solar radiation exergy accounting: Case study of Tunisia». In: Archives of Thermodynamics (2022), pp. 97–118 (cit. on p. 18).
[44] Sam Cross, Behnam Zakeri, David Padfield, and Sanna Syri. «Is battery energy storage economic in islanded power systems? Focus on the island of Jersey». In: 2016 13th International Conference on the European Energy Market (EEM). 2016, pp. 1–5. doi: 10.1109/EEM.2016.7521219 (cit. on pp. 19, 20).

[45] Johan Lindahl et al. «National survey report of PV power applications in Sweden». In: Uppsala University and International Energy Agency: Uppsala, Sweden 9 (2014) (cit. on p. 20).
[46] In: (). url: https://solargis.com/maps-and-gis-data/download/sweden (cit. on p. 20).
[47] Jennifer Leijon, Jens Engström, Malin Göteman, and Cecilia Boström. «De salination and wave power for freshwater supply on Gotland». In: Energy Strategy Reviews 53 (2024), p. 101404 (cit. on p. 21).
[48] Yunus Doğan and Ahmet Durap. «Summarizing data sets for data mining by using statistical methods in coastal engineering». In: World Academ Sci Eng Technol Int J Comput Inform Eng 11 (2017), pp. 643–648 (cit. on p. 22).
[49] European Commission. Photovoltaic Geographical Information System (PVGIS). Accessed: 2025-04-24. 2025. url: https://ec.europa.eu/jrc/en/pvgis (cit. on p. 30).
[50] Enrico Giglio, Ermando Petracca, Bruno Paduano, Claudio Moscoloni, Giuseppe Giorgi, and Sergej Antonello Sirigu. «Estimating the Cost of Wave Energy Converters at an Early Design Stage: A Bottom-Up Approach». In: Sustainability 15.8 (2023). issn: 2071-1050. doi: 10.3390/su15086756. url: https://www.mdpi.com/2071-1050/15/8/6756 (cit. on p. 37).
[51] In: (). url: https://solarduck.tech/ (cit. on pp. 40, 41).
[52] In: (). url: https://www.hydro.com/en/en/ (cit. on p. 41).
[53] Gobind Pillai and Husain Ali Yaqoob Naser. «Techno-economic potential of largescale photovoltaics in Bahrain». In: Sustainable Energy Technologies and Assessments 27 (2018), pp. 40–45. issn: 2213-1388. doi: https://doi.org/ 10.1016/j.seta.2018.03.003. url: https://www.sciencedirect.com/science/article/pii/S2213138817303703 (cit. on pp. 45, 47).
[54] Daniel Soto. «Modeling and measurement of specific fuel consumption in diesel microgrids in Papua, Indonesia». In: Energy for Sustainable Development 45 (2018), pp. 180–185. issn: 0973-0826. doi: https://doi.org/10.1016/j.esd.2018.06.013. url: https://www.sciencedirect.com/science/article/pii/S0973082618307403 (cit. on p. 46).
[55] In: (). url: https://www.globalpetrolprices.com/diesel_prices/ (cit. on p. 46).
[56] In: (). url: https://www.voronoiapp.com/energy/Whats-the-Average
Cost-of-1-kWh-Electricity-around-the-World--3398 (cit. on p. 46).
[57] In: (). url: https://euenergy.live/ (cit. on p. 46).
[58] Enrico Giglio, Ermando Petracca, Bruno Paduano, Claudio Moscoloni, Giuseppe Giorgi, and Sergej Antonello Sirigu. «Estimating the Cost of Wave Energy Converters at an Early Design Stage: A Bottom-Up Approach». In: Sustainability 15.8 (2023). issn: 2071-1050. doi: 10.3390/su15086756. url: https://www.mdpi.com/2071-1050/15/8/6756 (cit. on p. 48).

[59] In: (). url: https://ourworldindata.org/grapher/carbon-intensity electricity (cit. on p. 52).
[60] Abdul Qayoom Jakhrani, Andrew Ragai Henry Rigit, Al-Khalid Othman, Saleem Raza Samo, and Shakeel Ahmed Kamboh. «Estimation of carbon footprints from diesel generator emissions». In: 2012 International Conference on Green and Ubiquitous Technology. 2012, pp. 78–81. doi: 10.1109/GUT. 2012.6344193 (cit. on p. 52).
[61] Photovoltaics Report by Fraunhofer Institute for Solar Energy Systems ISE with the support of PSE Projects GmbH
Freiburg, 29 May 2025
www.ise.fraunhofer.de